

Review

Metal-Oxide Heterojunction: From Material Process to Neuromorphic Applications

Yu Diao , Yaoxuan Zhang, Yanran Li and Jie Jiang * 

Hunan Key Laboratory of Nanophotonics and Devices, School of Physics, Central South University, 932 South Lushan Road, Changsha 410083, China

* Correspondence: jiangjie@csu.edu.cn

Abstract: As technologies like the Internet, artificial intelligence, and big data evolve at a rapid pace, computer architecture is transitioning from compute-intensive to memory-intensive. However, traditional von Neumann architectures encounter bottlenecks in addressing modern computational challenges. The emulation of the behaviors of a synapse at the device level by ionic/electronic devices has shown promising potential in future neural-inspired and compact artificial intelligence systems. To address these issues, this review thoroughly investigates the recent progress in metal-oxide heterostructures for neuromorphic applications. These heterostructures not only offer low power consumption and high stability but also possess optimized electrical characteristics via interface engineering. The paper first outlines various synthesis methods for metal oxides and then summarizes the neuromorphic devices using these materials and their heterostructures. More importantly, we review the emerging multifunctional applications, including neuromorphic vision, touch, and pain systems. Finally, we summarize the future prospects of neuromorphic devices with metal-oxide heterostructures and list the current challenges while offering potential solutions. This review provides insights into the design and construction of metal-oxide devices and their applications for neuromorphic systems.

Keywords: metal oxide; heterojunction; memristor; transistor; neuromorphic applications



Citation: Diao, Y.; Zhang, Y.; Li, Y.; Jiang, J. Metal-Oxide Heterojunction: From Material Process to Neuromorphic Applications. *Sensors* **2023**, *23*, 9779. <https://doi.org/10.3390/s23249779>

Academic Editors: Athanasios Vourvopoulos and Serafeim Perdikis

Received: 29 October 2023
Revised: 30 November 2023
Accepted: 5 December 2023
Published: 12 December 2023



Copyright: © 2023 by the authors. Licensee MDPI, Basel, Switzerland. This article is an open access article distributed under the terms and conditions of the Creative Commons Attribution (CC BY) license (<https://creativecommons.org/licenses/by/4.0/>).

1. Introduction

Since the invention of the computer, technological progress has led to continuous improvements in computer performance and device function. Especially in recent years, the rapid technological developments for the Internet of Things and artificial intelligence (AI) have significantly increased the requirements for computer data processing [1–3]. Traditional von Neumann architectures could successfully solve the structural problem [4], but they encounter substantial challenges in contemporary computing, which are named the von Neumann bottleneck. At present, there are growing developments of new algorithms, such as artificial neural networks and deep learning [5,6]. Meanwhile, since the complementary metal-oxide semiconductor (CMOS) transistor may have reached its limit in terms of size, Moore’s law may begin to break down [7]. In contrast, the human brain, with a high parallelism, has a low power of 20 W because the average synaptic power consumption is only about 10 fJ [8–10]. Therefore, brain-inspired neuromorphic devices have attracted increasing interest as a potential solution for breaking the von Neumann bottleneck [11].

At the same time, metal-oxide materials may provide an ideal platform for the development of multifunctional neuromorphic devices due to their low power consumption, high stability, versatility, low cost, etc. [12–14]. Moreover, as basic building blocks, metal-oxide heterojunctions have an intriguing performance due to their higher charge mobility, lower leakage current, and faster response time ascribed to interfacial states and band bending [15–18]. Such heterojunctions allow the combination of different types of metal oxides

to achieve more functionalities and better performances. Therefore, neuromorphic devices based on metal-oxide heterojunctions may provide a great opportunity for next-generation computing technologies.

In this review, we first describe the various process methods of metal oxides and their heterojunctions. Then, we summarize the various devices and multifunctional neuromorphic applications based on metal-oxide materials and heterostructures, as shown in Figure 1. Finally, the key challenges and future directions are discussed for these kinds of neuromorphic devices. This review can provide a good understanding and guidance for entering the field of neuromorphic devices based on metal-oxide heterojunctions.

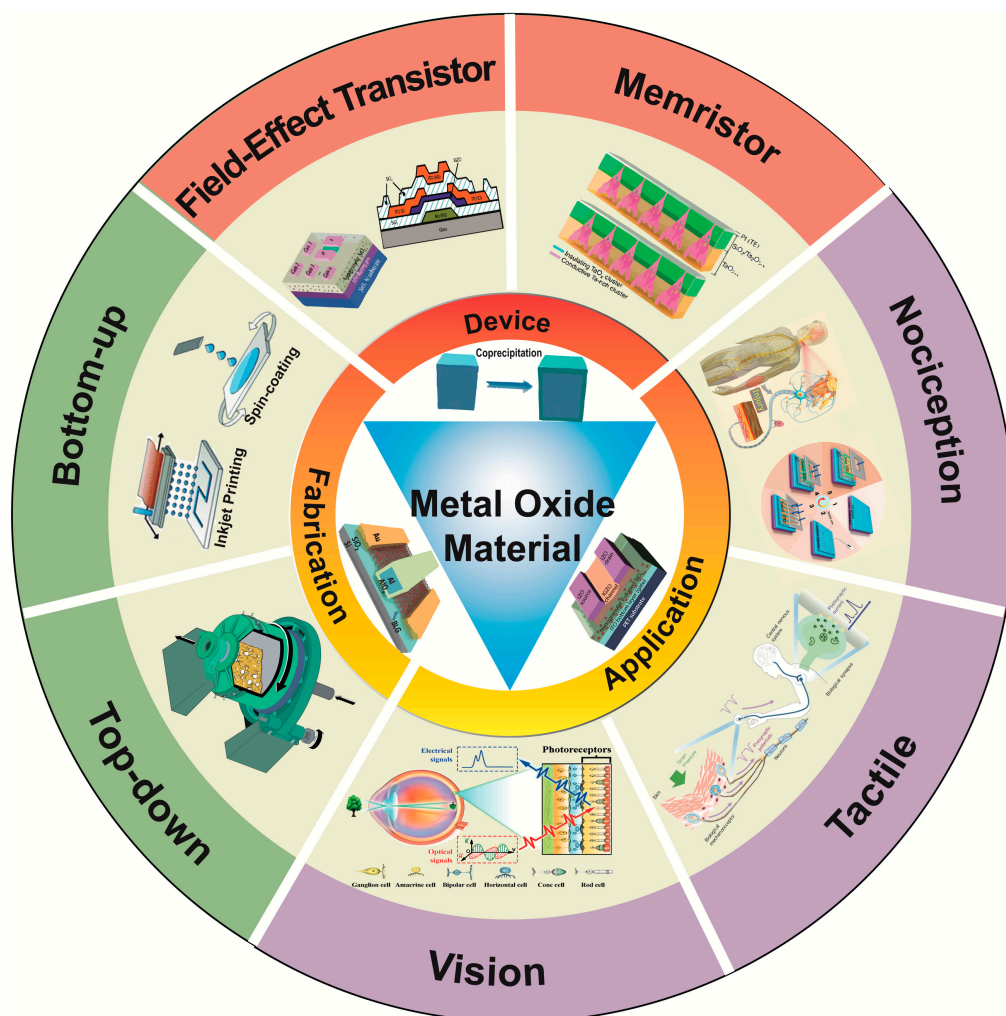


Figure 1. An overview of metal-oxide materials for neuromorphic applications. Reprinted with permission from [19]. Copyright 2023, IOP Publishing on behalf of the Chinese Physical Society. Reprinted with permission from [20]. Copyright 2021, Journal of Semiconductors. Reprinted with permission from [21]. Copyright 2020, American Chemical Society. Reprinted with permission from [22]. Copyright 1972, Royal Society of Chemistry. Reprinted with permission from [23]. Copyright 2021, Springer Nature. Reprinted with permission from [24]. Copyright 2019, John Wiley and Sons. Reprinted with permission from [25]. Copyright 2019, John Wiley and Sons. Reprinted with permission from [26]. Copyright 2021, John Wiley and Sons.

2. Metal-Oxide Heterojunction

2.1. Preparation of Metal-Oxide Materials

The synthesis and preparation of metal-oxide materials can be classified into two main categories: bottom-up and top-down approaches.

2.1.1. Bottom-Up Approaches

- **Solution-Deposition Method:** Solution-deposition methods include a variety of methods (Figure 2a). Solution techniques allow for the deposition of films at atmospheric pressure with minimal equipment cost. Scalable deposition methods that allow for uniform, large-area coverage are important for high-throughput industrial applications [22]. We highlight the sol-gel method and inkjet printing method in this section. The latter method mainly involves transforming the desired precursor material into an inkjet state and then distributing it for printing in the same way as other solution-deposition methods. A new kind of fully inkjet-printed InP/ZnSe QD/SnO₂ heterostructure thin film transistor (TFT) was fabricated with a bottom-gate, top-contact configuration by Liang et al. [27]. The fully printed device on a glass substrate exhibited a high optical transparency in the visible spectrum. This chemical method allows the formation of metal oxides using a colloidal solution (sol) approach. This method can well control composition and structure at the nanoscale. However, this process is always slow and often requires post-synthesis calcination [28].
- **Chemical Vapor Deposition:** Chemical vapor deposition is a process in which the substrate is exposed to one or more volatile precursors, and then reaction and decomposition are performed on the substrate surface to create the desired thin film. In typical CVD (Figure 2b), precursor gases are fed into the reaction chamber at ambient temperature. When they pass or come in contact with the heated substrate, they react or decompose to form a solid phase and then are deposited on the substrate. As shown in Figure 2c, the substrate temperature is very important and can affect the reactions that will take place. Compared to sol-gel methods, it typically offers a high degree of compositional and crystal structure control for precise material design. As a result, CVD has attracted growing interest in the semiconductor industry due to its large-area growth ability [29–31].
- **Electrodeposition:** Electrodeposition is a method for depositing ions from a solution onto an electrode's surface through an electrochemical reaction [32]. For example, Yin et al. easily prepared Cu₂O thin films using the electrodeposition method, thereby creating P-type Cu-based metal-oxide materials with excellent photoelectrochemical water splitting capability [32]. Unlike CVD, electrodeposition typically does not require high-temperature treatment or hazardous gases, making it environment-friendly. Moreover, it is a cost-effective way as it does not necessitate high-vacuum equipment or expensive precursors. These advantages make it an emerging favorite for the electronic materials [32,33].

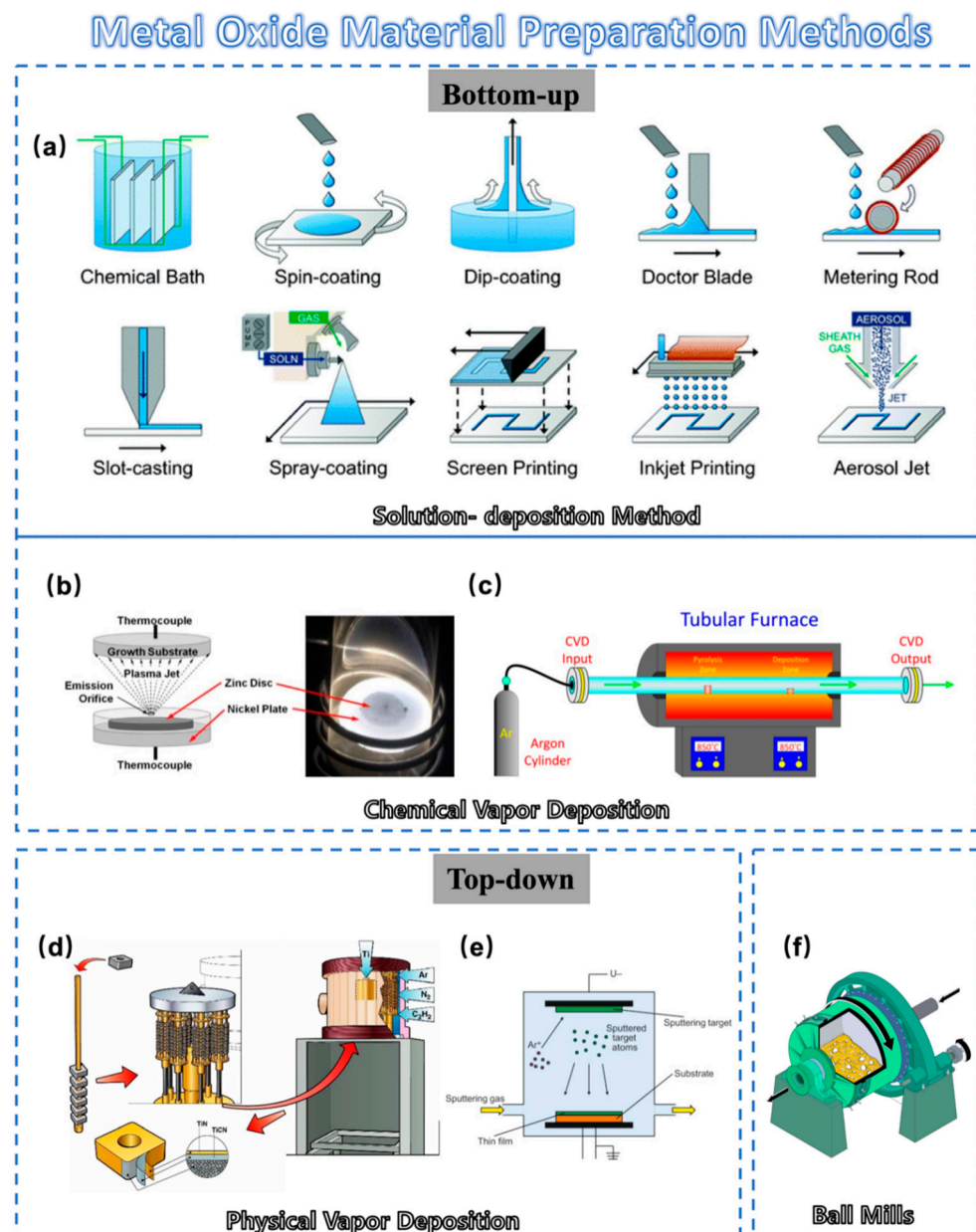


Figure 2. Schematic diagram of metal-oxide material preparation method: (a) Schematic of various solution-deposition processes: direct material growth without additional processing and liquid coating with additional processing to remove the solvent. Reprinted with permission from [22]. Copyright 1972, Royal Society of Chemistry. (b) Schematic cross-section of a thermal plasma chemical vapor deposition (CVD) system used to deposit ZnO nanocrystal thin films. Reprinted with permission from [34]. Copyright 2011, Springer Nature. (c) A scheme showing the setup used to grow carbon nanotubes inside nanoporous anodic alumina templates by CVD [35]. (d) Schematic diagram of conventional physical vapor deposition (PVD) process [36]. (e) Schematic illustration of the PVD process. Reprinted with permission from [37]. Copyright 2023, Elsevier. (f) A section cut-through of a ball mill. Reprinted with permission from [23]. Copyright 2021, Springer Nature.

2.1.2. Top-Down Approaches

- Mechanical Milling:** Mechanical milling is a very traditional and simple method of making metal-oxide powders. In this approach, metal-oxide powders are directly generated by mechanically grinding the bulk materials using a ball mill, as shown in Figure 2f. The electrical properties of metal oxides can easily be altered by adding other materials such as metals in this traditional method, as reported by Mikio et al. [38].

Using this method, Ag particles were added to $\text{Na}_x\text{Co}_2\text{O}_4$ thermoelectric oxide. A mechanical milling process was included for uniform dispersion of Ag particles in the $\text{Na}_x\text{Co}_2\text{O}_4$ matrix phase. Mechanical milling is also effective in reducing grain size, which is expected to affect the electrical resistivity and thermal conductivity of the product. However, it often lacks the capability of precise control over particle size distribution [38].

- **Physical Vapor Deposition:** As one of the most common processes on the market (Figure 2d), PVD offers distinct advantages compared to other methods for preparing metal-oxide materials [36]. It excels in its precision at the micro- and nanoscale, resulting in high-quality, uniformly dense films (Figure 2e). Moreover, PVD operates at lower temperatures, reducing the risk of thermal stress [39]. PVD films are high-purity, environment-friendly, and compatible with most materials and substrates. These attributes render PVD highly sought after in electronic/optical coatings and material enhancement [40,41]. PVD methods for preparing metal-oxide materials encompass magnetron sputtering, laser deposition, ion beam deposition, molecular beam epitaxy, thermal evaporation, etc. These techniques play an important role in preparing metal-oxide films with desired structural properties [42–47].

2.2. The Advantages of Heterojunctions

2.2.1. Types of Heterojunctions

We classify heterojunctions into all-organic heterojunctions, mixed organic–inorganic heterojunctions, and all-inorganic heterojunctions based on the type of material. All-organic heterojunctions usually have better processability and bendability [48], and substrate selection and growth techniques play a large role in achieving the desired material properties [49]. With high stability and high electron mobility, all-inorganic heterojunctions allow for device performance and are less flexible. These materials usually require high temperatures or complex preparation processes. Organic–inorganic hybrid heterojunctions combine the processability of organic materials with the high stability and high electron mobility of inorganic materials [50]. This structure allows for a better balance of electron and hole transport, improving the performance of electronic devices. However, the combination of such heterojunctions often requires a high degree of matching [51]. The choice of which heterojunction to use depends largely on the needs of the particular application, such as flexibility, stability, processing difficulty, and cost. Due to the presence of some micro/nano interactions such as surface and interface engineering, quantum confinement effects, strain engineering, chemical interactions, and doping [52–56], all kinds of heterojunctions have something in common; that is, the formation of heterojunctions allows the material properties to be improved dramatically, which is the basis of why heterojunctions involving metal oxides can be used in a wide range of applications, and this provides enlightenment for metal-oxide heterojunctions in neuromorphic applications.

2.2.2. Applications of Heterojunctions

We have already introduced the superior properties of heterojunctions, and when metal-oxide materials are involved in heterojunctions, they often have their own unique advantages. In this section, we will introduce the properties and applications of heterojunctions with the participation of metal oxides in some common areas.

- Electrode materials for supercapacitors (SCs)

In recent years, transition-metal oxides (TMOs) have often been considered as the main cathode material for supercapacitors because of their versatile redox reactions, high theoretical capacitance, and economic feasibility [57,58]. However, TMOs always possess relatively low electrical conductivity, which leads to poor electrochemical performance, such as low specific capacitance, rate performance, and cycling stability [59].

Zhang et al. proposed a unique ZNCS/ZNCO heterostructure (Figure 3a) obtained by vulcanization of ZNCO for positive electrodes of SCs [60]. The resulting flower-like ZNCS/ZNCO composite exhibits several noteworthy advantages, including excellent

conductivity, robust structural stability, and enhanced redox reactions. Therefore, the incorporation of oxide heterostructures has a positive impact on the performance of SCs.

Properties and Applications of Metal-Oxide Heterojunctions

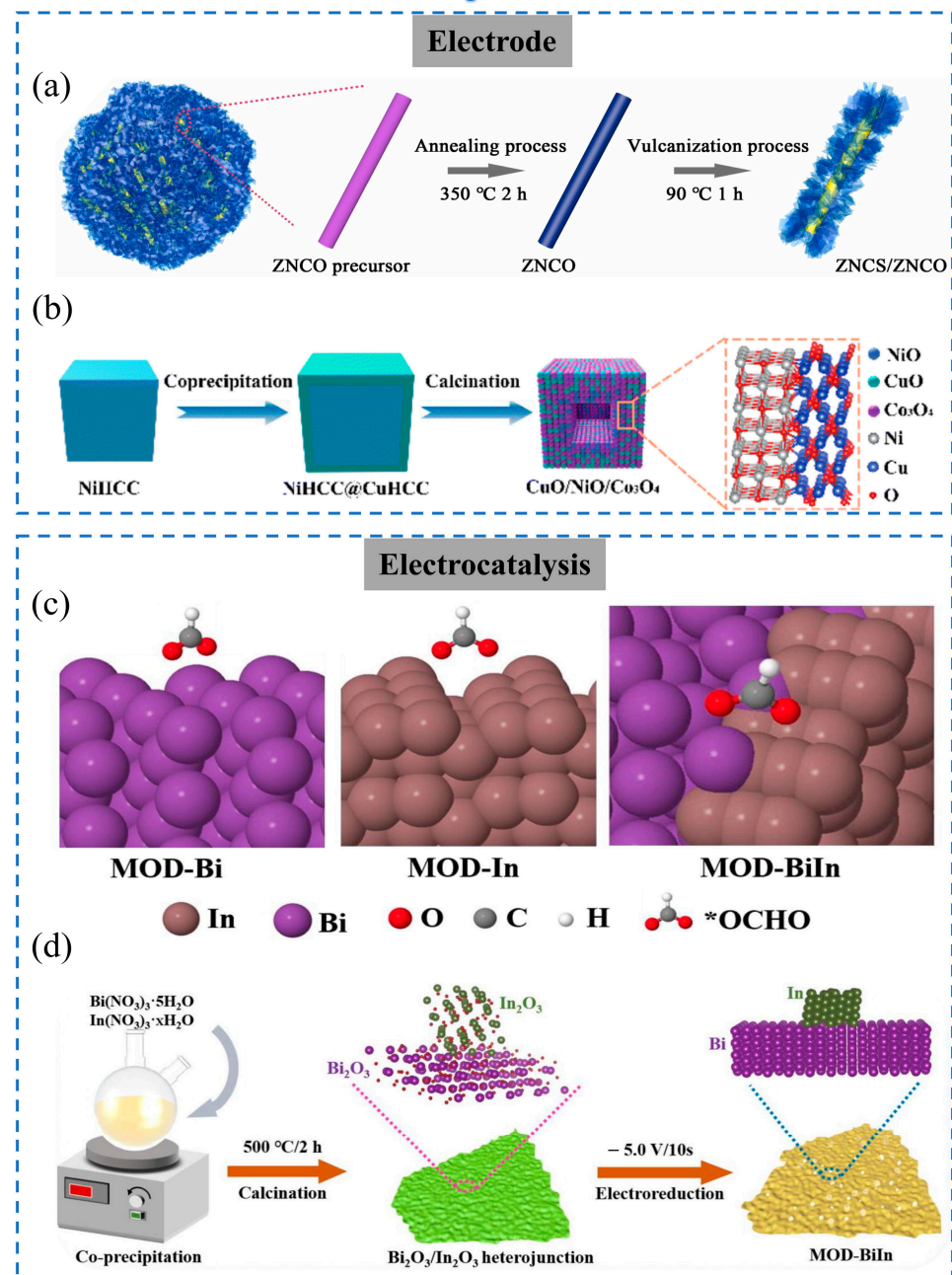


Figure 3. Schematic diagram of the preparation method for metal-oxide heterojunction and its applications: (a) Schematic formation process of ZNCS/ZNCO heterostructure composites. Reprinted with permission from [60]. Copyright 2023, Elsevier. (b) Schematic diagram of the procedure for a hollow CuO/NiO/Co₃O₄ heterostructure. Reprinted with permission from [61]. Copyright 2003, Royal Society of Chemistry. (c) The illustration of the fabrication process for Bi₂O₃/In₂O₃ heterojunction (MOD-BiIn) hybrid material. (d) The overview schematic of *OCHO on MOD-Bi, MOD-In, and MOD-BiIn surfaces. Reprinted with permission from [62]. Copyright 2023, Elsevier.

In another work, Ju et al. proposed a ternary hollow CuO/ NiO/Co₃O₄ heterostructure (Figure 3b) [61]. In this work, core–shell-structured Prussian blue analogs (PBAs) (NiHCC@CuHCC) with Ni-based PBAs (NiHCC) as the core and Cu-based PBAs (CuHCC) as the shell were prepared using the crystal seed method. The enhanced electrochemical performance could benefit from the following characteristics: (1) The hollow structure can provide more active sites, reduce the structural strain, and keep the electrode from collapsing. (2) The electronic structure of CuO/NiO heterojunction can be well tuned and finally facilitate the electron/ion migration [61].

In general, the synergetic effect between various metal oxides in a heterostructure facilitates electron/ion migration. More importantly, heterostructures often combine the advantages of all materials to achieve multiple advantages in various physical and chemical properties [61,63,64].

- Excellent properties for electrocatalysis

The unique features of metal-oxide heterojunctions also confer substantial advantages in electrocatalytic applications. This section will elucidate the merits of metal-oxide heterojunctions in electrocatalysis.

Traditionally, catalysts with high CO₂ reduction reaction (CO₂RR) selectivity have relied on weak metal–hydrogen bonds to suppress hydrogen evolution reaction activity [65–67]. In recent years, materials derived from metal oxides or sulfides have been found to exhibit better electrocatalytic activity than their corresponding pure metal counterparts [68,69]. Specifically, Bi-based materials such as Bi-MOF, Bi₂O₃, or Bi₂O₂CO₃ are commonly used as precursors for efficient electrocatalysts. However, these metal-oxide materials do not enhance the performance or maintain high selectivity [62]. However, indium-based metal-oxide heterojunctions can promote selectivity, especially when indium atoms are introduced at the metal sites of a heterojunction (Figure 3c) [70–72].

As shown in Figure 3d, Ye et al. synthesized a material containing partial bimetallic oxides (In_xBi_{2-x}O₃) and heterojunctions (In₂O₃-Bi₂O₃) [62]. In this work, it was shown that heterojunctions can improve performance while maintaining high formate selectivity. This demonstrated that metal-oxide heterostructures have great potential for electrocatalysis. Furthermore, the role of heterojunctions can be also considered as an enlightening contribution in neuromorphic applications.

3. Neuromorphic Devices Based on Metal-Oxide Heterojunctions

3.1. Biological Synapses and Synaptic Plasticity

Neurons are interconnected by synapses. A synapse specifically connects the axonal terminals of the presynaptic neuron and postsynaptic neuron, thus completing the information transmission between nerve cells [8]. The structure of the human brain is complicated, with ~10¹⁵ synapses and ~10¹¹ neurons [8,73,74].

Synaptic plasticity is an important feature of synapses. It is often considered to be the major cellular mechanism for learning and memory [75]. According to the duration, synaptic plasticity can be divided into short-term plasticity and long-term plasticity. Short-term plasticity has a shorter duration of action, typically tens of milliseconds to minutes. Long-term plasticity, including long-term potentiation (LTP) and long-term depression (LTD), can last much longer, from tens of minutes to even some days [76]. Meanwhile, the conversion between LTP and LTD allows for the easy regulation of synaptic weights [77,78]. In the work of Liu et al., artificial devices with Li-AlO_x ion electrolytes were proposed [79], and the short-term potentiation (STP) and LTP emulations of the synaptic weight modulation by the ion electrolyte were emulated based on the electrostatic coupling of Li ions in the electrolyte and electrochemical doping with the metal-oxide In₂O₃, respectively [80,81]. After the gate-electrolyte stimulus, the diffusion of the accumulated ions in the electrolyte as the result of the gradient potential leads to the decay of the channel current to the resting level, emulating STP behavior. Electrical stimulus with higher amplitudes or long durations induces electrochemical doping, leading to an LTP behavior of the synaptic weight [9].

Normally, memory is divided into two categories by duration: short-term memory (STM) and long-term memory (LTM). In the process of consolidating LTM, STM processes are responsible for cognition. STM can be converted into LTM. STM can be achieved by the continuous firing of neurons [82]. It is believed that LTM is related to the change in the probability of neurotransmitter release by presynaptic neurons, the change in the sensitivity of postsynaptic neuronal receptors to neurotransmitters, and the change in synaptic structure and synthesis of new proteins [83]. The relationships and properties of LTM and STM need to be further studied. That is why it is important to fabricate devices capable of regulating pre- and post-synapses in synaptic electronics.

Emerging metal-oxide heterojunctions can provide a good opportunity for developing brain-inspired neuromorphic devices. Neuromorphic metal-oxide heterojunction devices can be classified as two-terminal memristors and three-terminal transistors. In the following section, we provide a brief description of the working mechanisms of these different device structures.

3.2. Two-Terminal Devices Based on Metal-Oxide Heterojunctions

- Forming conducting filaments

Two-terminal synaptic devices, also known as memristors, have resistive states that depend heavily on past states, which opens up the possibility of emulating synaptic connections between neurons. The typical device structure is based on a metal-oxide resistive switching layer sandwiched between two metal electrodes [84,85], as shown in Figure 4a. A “SET” voltage switches the device from a high-resistance state to a low-resistance state due to the electrically generated oxygen vacancies (V_o) in the metal-oxide layer. In contrast, a “RESET” voltage switches the device from a low-resistance state to a high-resistance state due to the restoration of the V_o [86,87]. In general, after the SET process, one or more conductive filaments are formed in the oxide layer, while some of the conductive filaments are broken after the RESET process [88].

Moreover, metal-oxide heterojunctions can tune the filament microstructure by controlling the growth and dissolution rates. Wang et al. proposed a resistive switching device by introducing a SiO_2 ion diffusion limiting layer (DLL) at the TiN/TaO interface (Figure 4b,c) [89]. The device architecture consisted of a multi-layered Pt/TiN/ SiO_2 /TaO_x/Pt stack. The DLL layer led to more linear conductance changes and holds high promise for neuromorphic applications [90].

- Vacancy migration

The relatively high mobility of oxygen-related defects can also be used as an important method for adjusting the synaptic weights in memristors. Oxygen anion migration under an external electric field is one of the main resistive switching phenomena [21]. Dmitri B. Strukov et al. introduced a physical model for Pt/TiO₂/Pt devices [77,91]. As reported by Hansen et al. in 2015, Al/Al₂O₃/Nb_xO_y/Au double-barrier memristors were proposed for the optimization of electron tunneling [92] and ion diffusion [89]. Two models used to describe the double-barrier tunnel junctions are shown in Figure 4d,e. This migration enables nuanced, area-dependent resistance modulation. These studies highlight the critical role of vacancy migration in achieving precise control over electrical conductance, laying the groundwork for more stable and efficient artificial synapses [90].

3.3. Three-Terminal Devices Based on Metal-Oxide Heterojunctions

While memristors primarily focus on information storage and plasticity, the conductance of neuromorphic field-effect transistors (FETs) can be well controlled through the three terminals [93]. In fact, the gate electrode in a transistor can be viewed as the presynaptic membrane, while the channel layer can be treated as the postsynaptic membrane [94–96]. The presynaptic stimulus is a spike input from the gate electrode, and the change in channel conductance is used to emulate the excitatory postsynaptic current [79,93]. Furthermore, synaptic characteristics such as paired-pulse facilitation (PPF), LTP, and LTD can be easily observed in heterostructures for neuromorphic computing [97].

Herein, we categorize metal-oxide FETs based on the device architecture with two types, namely top-gate and bottom-gate FETs, as detailed in the following section.

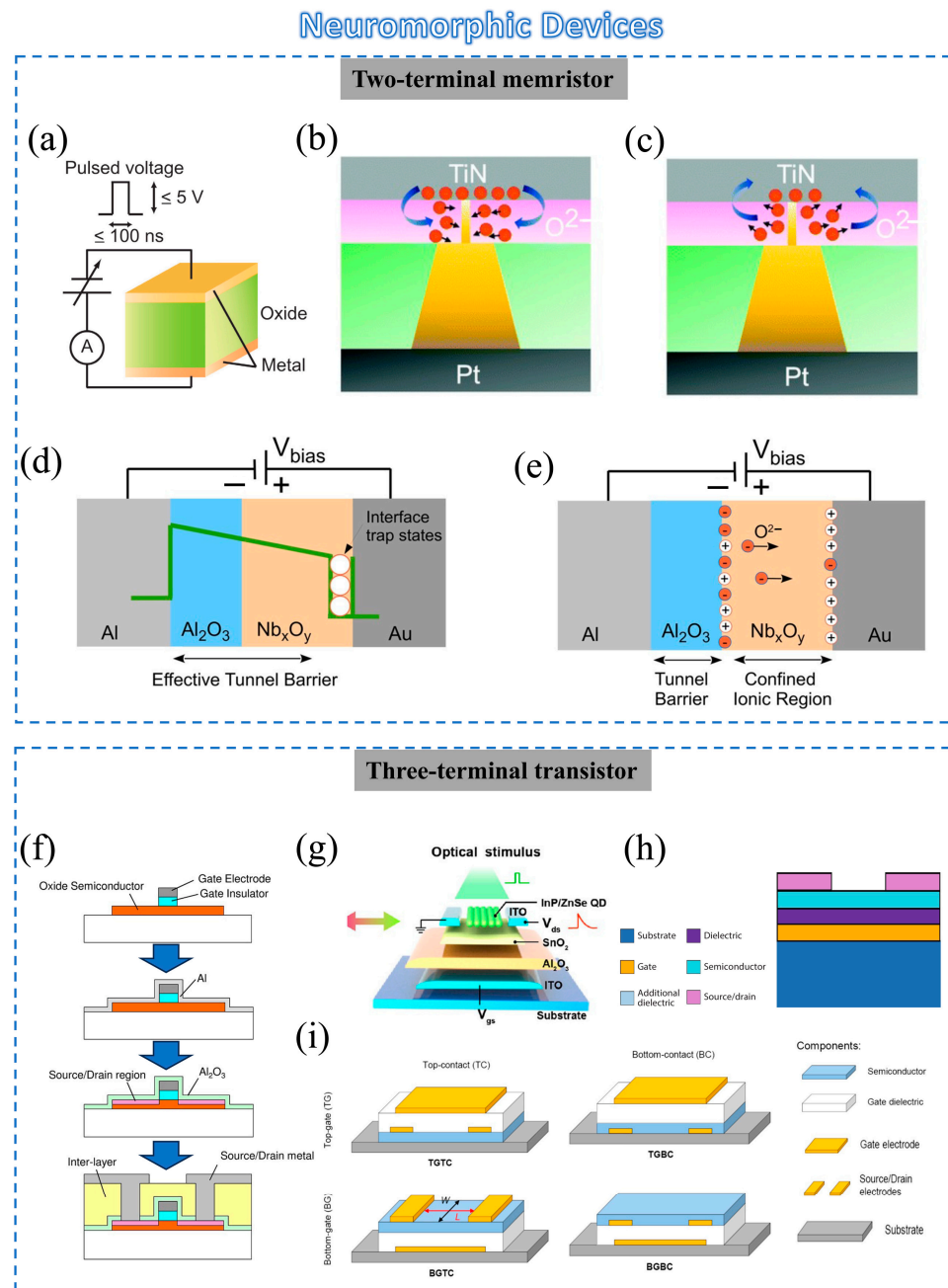


Figure 4. (a) Diagram of a resistance random access memory cell with a capacitor-like structure. Reprinted with permission from [84]. Copyright 2008, Elsevier. Schematic of filament (b) growth and (c) dissolution dynamics. Reprinted with permission from [89]. Copyright 2009, RSC Pub. (d,e) Two models describing the memristive double-barrier tunnel junctions. (d) Simplified cross-sectional view of the memristive tunnel junctions. (e) An alternative model to (d) [92]. (f) Process flow for fabrication of a self-aligned top-gate oxide TFT. Reprinted with permission from [98]. Copyright 2013, John Wiley and Sons. (g) Schematic structure of the InP/ZnSe quantum dot (QD)/ SnO_2 hybrid TFT. Reprinted with permission from [27]. Copyright 2022, American Chemical Society. (h) Schematic diagrams of the device structures with bottom gate. Reprinted with permission from [20]. Copyright 2015, IEEE. (i) Scheme of the four transistor structures: top gate, top contacts (TGTC); top gate, bottom contacts (TGBC); bottom gate, top contacts (BGTC); bottom gate, bottom contacts (BGBC). Reprinted with permission from [99]. Copyright 2020, American Chemical Society.

3.3.1. Bottom-Gate FETs

Bottom-gate FETs have the simplest device structure. For example, the production of the BGBC structure shown in Figure 4h just needs one lithographic step, which makes the device fabrication relatively quick and cheap [20]. The bottom-gated three-terminal FETs proposed by Rehman et al. are auspicious candidates for the emulation of biological functions in realizing proficient neuromorphic computing systems [100]. These devices exploit the hysteresis effect in the transfer curves of that kind of FET to explore excitatory/inhibitory post-synaptic currents (EPSCs/IPSCs), LTP, LTD, spike timing/amplitude-dependent plasticity (STDP/SADP), and PPF.

As a special kind of FET, TFTs were first fabricated in 1962 by Paul K. Weimer, and in 1979, the first functional TFT was successfully demonstrated [101,102]. Oxide-based TFTs were first reported in 1964 by Klasens et al., and then the most famous indium gallium zinc oxide TFT was proposed by Nomura et al. in 2004 [103,104]. Oxide TFTs have obvious advantages: high mobility, good stability, nice chemical resistance in liquids, high transparency, and ease of processing [94,105,106].

In some research, managing vacancies has proved important for improving the performance and stability of oxide TFTs, particularly in heterojunction configurations. Liang et al. [27] proposed a structure of InP/ZnSe QD/SnO₂ hybrid TFTs using full printing technology. In this structure (Figure 4g), the band alignment near the heterojunction resulted in the effective separation of photogenerated electrons and holes, which resulted in a spectrally dependent response in photonic synaptic devices. Using both the high photosensitivity of InP/ZnSe QDs and the high electron mobility of SnO₂, the devices could well emulate key synaptic behaviors such as EPSC, STP, LTP, and PPF. An artificial vision system was finally demonstrated with enhanced image recognition and processing efficacy. These findings underscore the viability of employing such heterojunction devices for optoelectronic synapses and also offer a scalable fabrication strategy for advanced artificial vision systems [27].

3.3.2. Top-Gate FETs

As for the top-gate structure, the fabrication process involves the channel structure, followed by the gate dielectric and gate electrode (Figure 4f) [98]. In this structure, the current flows effectively at the top interface of the semiconductor. The semiconductor layer is encapsulated by dielectric and gate electrodes, protecting it from damage in subsequent processing steps.

However, at the same time, the semiconductor may be also affected by thermal cycling and solvents in subsequent process steps, potentially deteriorating the transistor performance. When a sintering step is employed, a bottom-gate structure may be more suitable. This is because subsequent sintering steps can degrade the semiconductor performance in top-gate transistors. Although top-gate and bottom-gate structures have their own exquisite manufacturing technology, they all play an important role in neuromorphic applications [107].

4. Neuromorphic Applications

In the actual activity of life, the sensory nervous system is formed by various neural networks and circuits connected by synapses with neurons as the basic unit. Neuromorphic devices with metal-oxide heterojunction have attracted increasing interest and become a hot topic in recent years. In the following sections, we summarize the recent progress for these neuromorphic devices in visual, tactile, and nociceptive systems.

4.1. Neuromorphic Visual System

The visual nervous system is an essential way for humans to acquire external information, more than 80% of which is obtained by vision [108]. In the nervous system, when incident light enters the eyeball, optic nerve fibers in the retina convert external signals into biological signals and transmit action potentials to the visual cortex in the brain to form

vision, as shown in Figure 5a [109–111]. Figure 5b illustrates a method of emulating the human visual nervous system using neuromorphic devices [112].

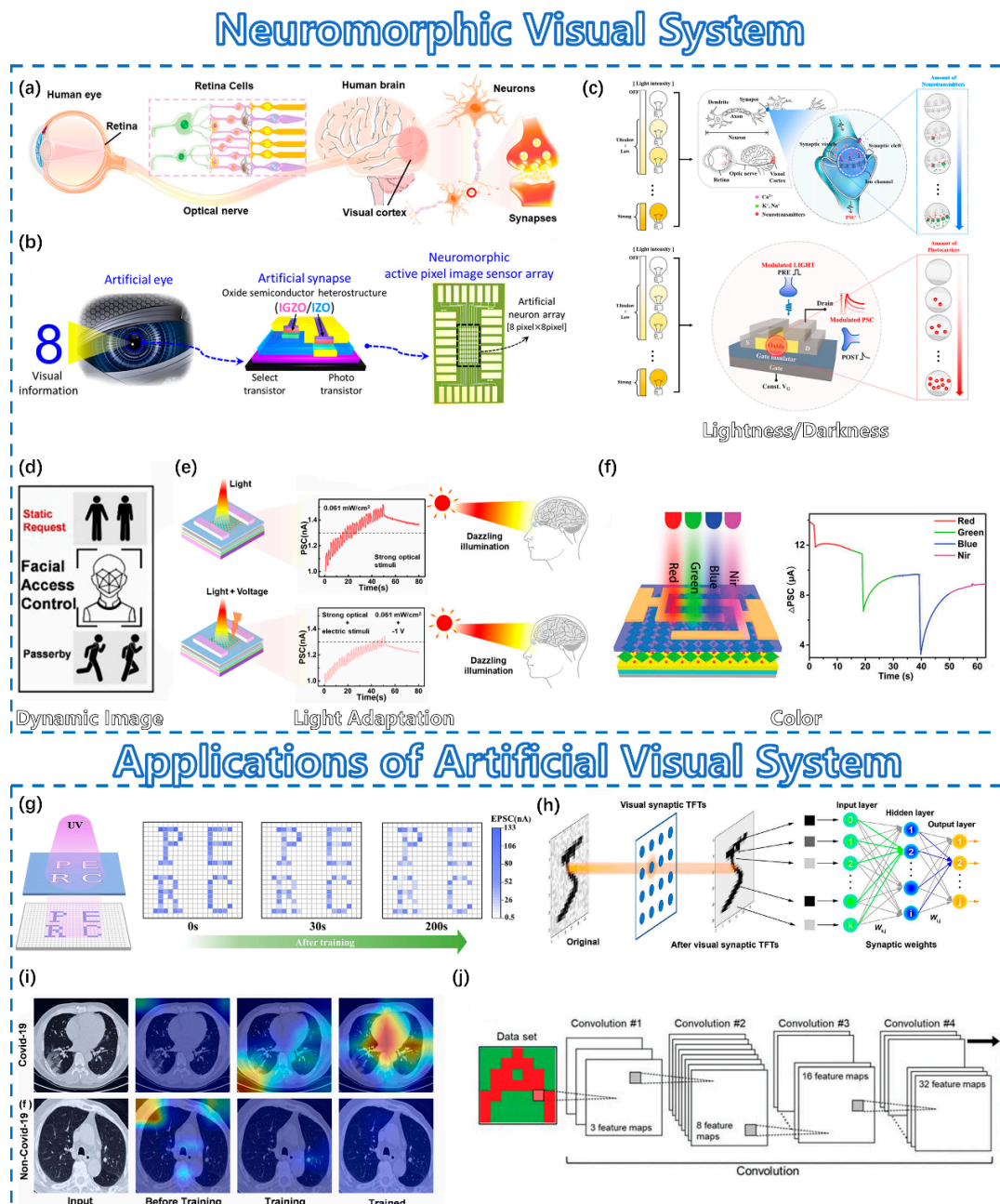


Figure 5. Neuromorphic visual system. (a) Schematic diagram of the human visual system. Reprinted with permission from [109]. Copyright 2022, American Chemical Society. (b) Schematic diagram of artificial visual system. Reprinted with permission from [112]. Copyright 2021, American Chemical Society. Some typical visual features: (c) Lightness and darkness. Reprinted with permission from [109]. Copyright 2022, American Chemical Society. (d) Dynamic image [113]. (e) Light adaptation. Reprinted with permission from [114]. Copyright 2022, Elsevier. (f) Color perception. Reprinted with permission from [115]. Copyright 2021, John Wiley and Sons. Several applications of artificial visual systems: (g) Visual information learning and memory processing. Reprinted with permission from [27]. Copyright 2022, American Chemical Society. (h) Image preprocessing. Reprinted with permission from [79]. Copyright 2022, Elsevier. (i) Image recognition. Reprinted with permission from [116]. Copyright 2022, John Wiley and Sons. (j) Color pattern recognition. Reprinted with permission from [117]. Copyright 2023, Royal Society of Chemistry.

The visual system under lightness/darkness conditions can be successfully emulated as shown in Figure 5c. When a signal is transmitted to the terminal of the presynaptic neuron, the electrical signal is converted into a chemical signal and accompanied by the release of neurotransmitters, which can bind to the receptors of the postsynaptic neuron to complete the signal transmission between neurons. When artificial synapses are stimulated by external light, the number of photocarriers can be increased to tune the device conductance, which is similar to the function of neurotransmitters in the actual nervous system. Therefore, the photoresponse of artificial synapses is weaker in the dark than in sufficient light, which is very consistent with human visual neural behaviors [113]. This helps neuromorphic devices to capture both static and dynamic images, as shown in Figure 5d [114]. Under bright light, a photoreceptor with rod and cone cells will adapt to external light and then produce the appropriate level of electrical spikes according to the ambient light intensity, which is known as light adaptation [118,119]. By introducing a negative voltage pulse, a neuromorphic device can adapt to light and avoid possible damage from strong light, as shown in Figure 5e [109]. At the same time, a neural network can reduce the response of nerve impulses near the target, and color recognition can be demonstrated [120]. Different neuromorphic devices can be designed to realize light absorption for the recognition of different colors, as shown in Figure 5f [115,116,121,122]. Different visual functions can be successfully demonstrated, such as visual information learning/memory, image preprocessing, and color pattern recognition [27,79,116,117].

4.2. Neuromorphic Tactile System

Skin, as the largest sensory organ in the human body, plays an important role in the actual interaction process. It is embedded with countless tactile receptors, helping the body to complete a series of complex physical interactions, such as snatching, sliding, and the judgment of object properties [123]. The basic principle of the human tactile nervous system is shown in Figure 6a. An artificial tactile nervous system may be a powerful way to realize the future of bionic robots. So far, various ways to implement these systems have been reported, including the use of piezoelectric, piezophototronic, piezoresistive, capacitive, deformable ionic dielectric, and triboelectric materials, as detailed below.

(i) Piezoelectric materials generate an electrical potential when the pressure/stress changes, which achieves the conversion of mechanical signals to electrical signals, as shown in Figure 6b [124,125]. (ii) The piezophototronic effect is that the interface band structure is effectively modulated by a piezoelectric polarization charge caused by external stress [126]. A piezophototronic material can be used in a light-emitting diode array of pixels, resulting in a nice pressure distribution, as shown in Figure 6c [127]. (iii) The resistance of a piezoresistive material will change with external pressure or stress. Consequently, piezoresistive materials could be deployed as tactile receptors to detect mechanical stress or pressure, as shown in Figure 6d. This change in resistance largely comes from the variation in the conductive path or structure of the material itself. Wang et al. fabricated a carbon nanotube paper film (CNTF)/stress-induced square frustum structure (SSFS) pressure sensor with ultra-sensitive and wide-range flexible performance. An external effect will change the inner conductive path of the sensor, which is composed of contacts between interdigital electrodes (IDEs) and fibers inside the CNTF as well as contacts between fibers themselves [128]. Cheng et al. developed sensors based on Au/graphene composite films (AGCFs) with hierarchical cracks. By using electrical resistance varying with the change in crack number and areas, the sensing performance presents high sensitivity, excellent linearity, and adjustability due to tuning pattern regulation [129]. (iv) For capacitive tactile receptors, external effort usually causes a change in the thickness of the dielectric layer, which affects the conductive value, mimicking skin, as shown in Figure 6e. Recently, there has also been great interest in utilizing 4D printing devices to fabricate capacitors to be used in physiological monitoring sensors [130]. (v) In a deformable ionic dielectric, external pressure will effectively force ions accumulated at the interface between the semiconductor and dielectric to influence the current level, as shown in Figure 6f. (vi) As for triboelectric

receptors, the principal mechanism is the triboelectric nanogenerator (TENG). In devices, the variation in two layers in the TENG will cause the motion of electrons to modulate the gate voltage, as shown in Figure 6g. Tactile devices with the various principles above have been developed, and their functions in neuromorphic tactile systems are endless.

Figure 6h shows a prosthetic hand with tactile sensors that can transform mechanic signals into nervous signals. Although only three tactile sensors are integrated per finger, they can still help amputees feel pain and distinguish shapes [131]. As shown in Figure 6i, tactile devices with high sensitivity to pressure can be utilized to help blind people learn braille or recreate the sense of touch [132]. Since a capacitive tactile device is highly sensitive to distance, fingerprint recognition was successfully realized, as shown in Figure 6j [133]. In addition, the typical functions of tactile neurons can be emulated to perceive dynamic pressures with different intensities, sizes, and frequencies, as shown in Figure 6k [134]. Tactile devices have many promising applications, as shown in Figure 6l for physiological signal detection [135], Figure 6m for recognition of three gestures [136], Figure 6n for monitoring human motions [137], and Figure 6o for near-sensor analog computing [24].

4.3. Neuromorphic Nociceptive System

Tactile perception is one of the primary methods by which the human body coordinates and interacts with its surroundings. At the same time, touch operation is also the primary way of human–computer interaction. Human skin is covered with different types of mechanoreceptors. When the skin senses changes in pressure, temperature, or humidity in the external environment, it sends out tiny electrical signals that are transmitted to the brain with nerve fibers, which in turn produce the sense of touch [138]. The combination of tactile sensors and synaptic devices provides a solution for implementing neuromorphic functions for strain pattern recognition and processing [24]. As critical sensory components in the nervous system, nociceptors can recognize noxious stimuli collected from tactile sensory signals and transmit signals to the central nervous system, enabling a response that avoids damage to the body, as shown in Figure 7a [139]. Figure 7b shows the characteristics of the nociceptive nervous system. There are several basic characteristics in the nociceptive system [140–145]: (i) Threshold behavior means that a significant response appears until the external stimulus approaches or even exceeds the threshold value, as shown in Figure 7c. (ii) Relaxation behavior means that nociceptors can maintain an extremely high response after the removal of stimuli, as shown in Figure 7d. (iii) Hyperalgesia and allodynia behaviors indicate an enhanced response to noxious stimuli is generated even below the stimulus threshold, as shown in Figure 7e. (iv) Adaption means that nociceptors will not respond to dangerous stimuli, as shown in Figure 7f [146].

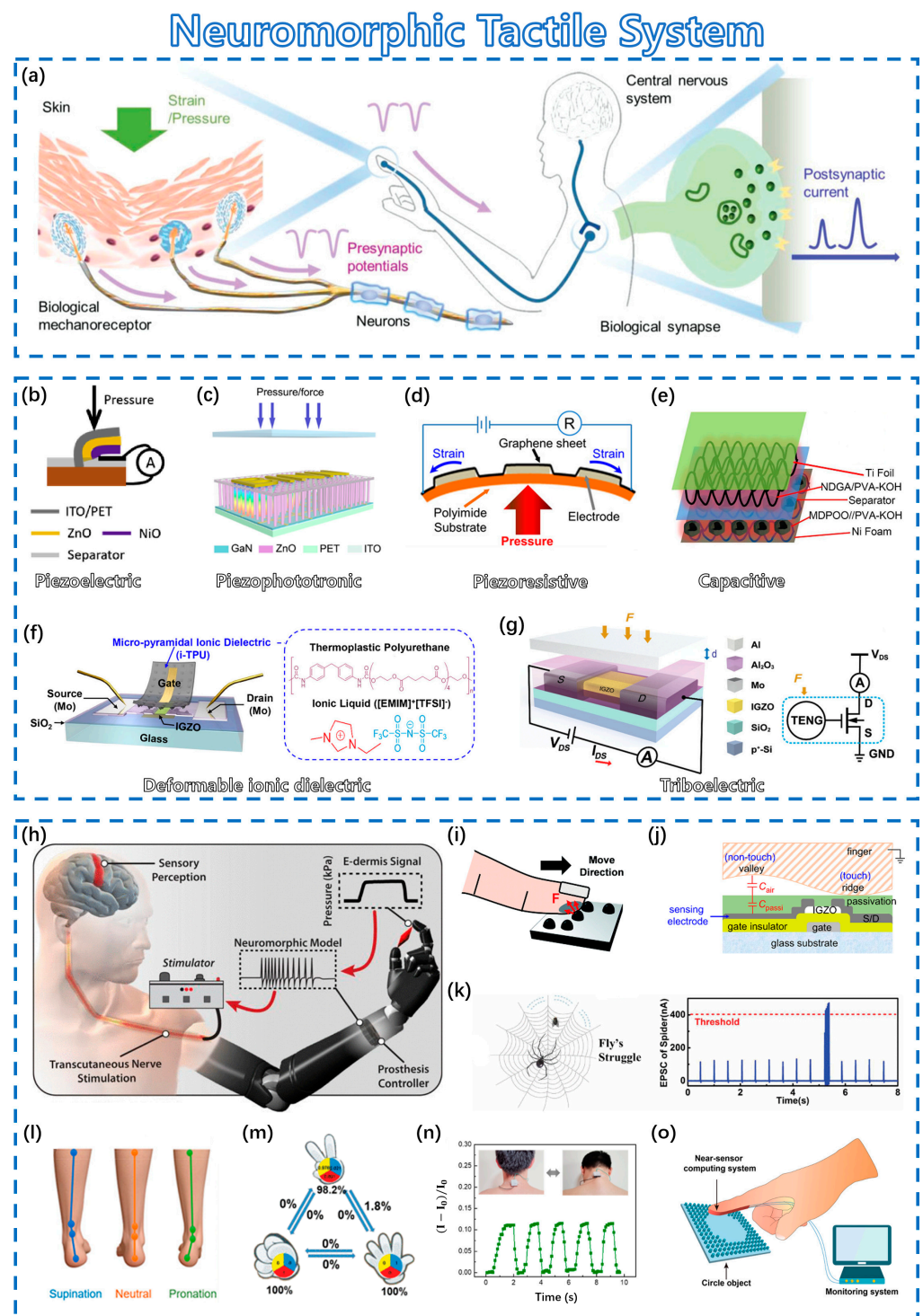


Figure 6. Neuromorphic tactile system. (a) Schematic diagram of the human tactile nervous system. Reprinted with permission from [24]. Copyright 2019, John Wiley and Sons. Sensing mechanisms: (b) Piezoelectric. Reprinted with permission from [125]. Copyright 2020, Elsevier. (c) Piezophototronic. Reprinted with permission from [127]. Copyright 2019, Elsevier. (d) Piezoresistive. Reprinted with permission from [147]. Copyright 2020, John Wiley and Sons. (e) Capacitive. Reprinted with permission from [148]. Copyright 2018, American Chemical Society. (f) Piezocapacitive. Reprinted with permission from [149]. Copyright 2020, John Wiley and Sons. (g) Triboelectric. Reprinted with permission from [150]. Copyright 2017, American Chemical Society. Applications of neuromorphic tactile systems: (h) Prosthesis with tactile sensor feedback. Reprinted with permission from [131]. Copyright 2019, IEEE. (i) Touching convex Braille numbers. Reprinted with permission

from [132]. Copyright 2012, Royal Society of Chemistry. (j) Touch-fingerprint sensor. Reprinted with permission from [133]. Copyright 2018, John Wiley and Sons. (k) Mechanical sensory mechanism. Reprinted with permission from [134]. Copyright 2020, IEEE. (l) Physiological signal detection. Reprinted with permission from [135]. Copyright 2018, American Chemical Society. (m) Recognition of three gestures. Reprinted with permission from [136]. Copyright 2019, IEEE. (n) Monitoring human motions. Reprinted with permission from [137]. Copyright 2023, American Chemical Society. (o) Near-sensor analog computing system. Reprinted with permission from [151]. Copyright 2022, John Wiley and Sons.

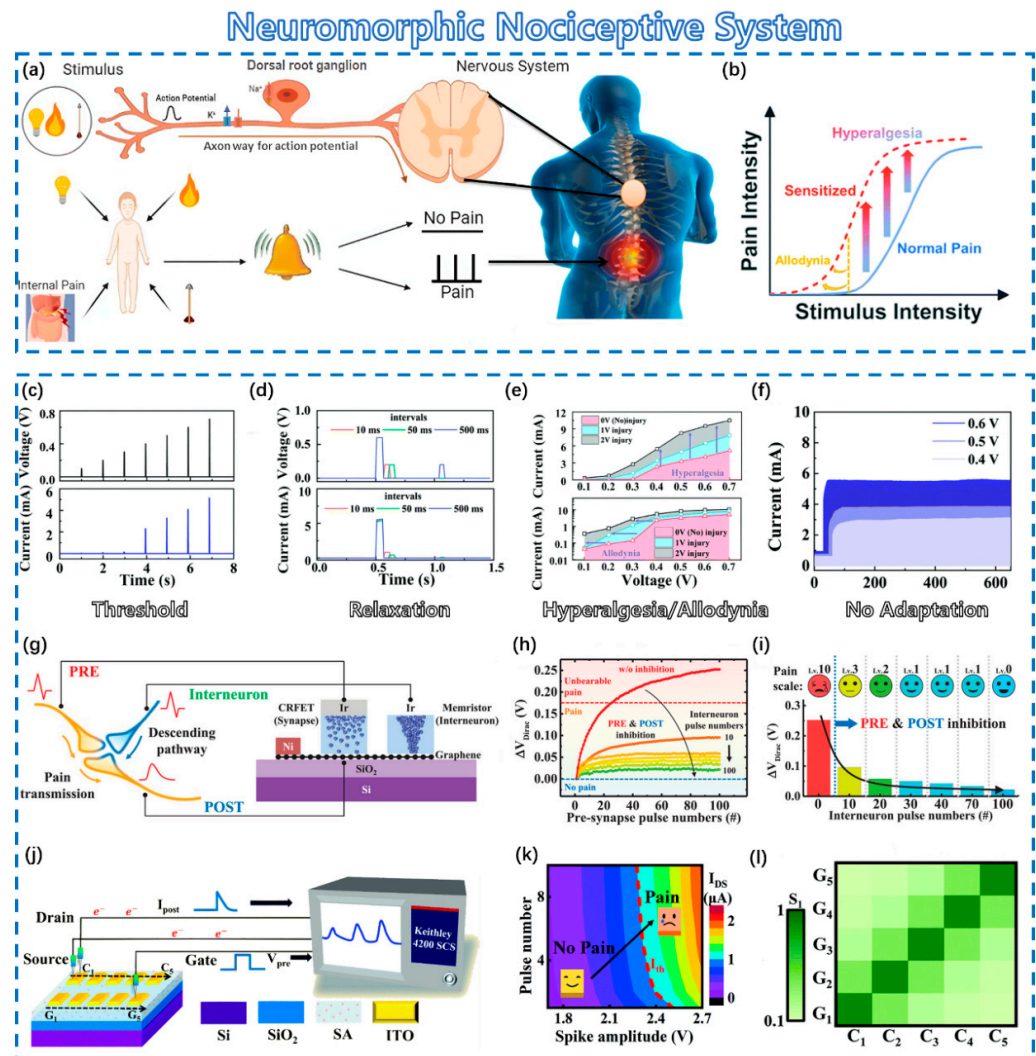


Figure 7. Neuromorphic nociceptive system. (a) Schematic diagram of human nociceptive nervous system. Reprinted with permission from [139]. Copyright 2009, Royal Society of Chemistry. (b) Characteristics of nociceptive nervous system: (c) threshold, (d) relaxation, (e) allodynia/hyperalgesia, (f) no adaptation. Reprinted with permission from [146]. Copyright 2012, Royal Society of Chemistry. Artificial pain modulation system: (g) schematic diagram, (h) pain inhibition in the artificial tactile nervous system, and (i) inhibition abilities. Reprinted with permission from [152]. Copyright 2022, John Wiley and Sons. Graded pain perception: (j) oxide transistor arrays and test system, (k) evaluations of pain-perception behaviors, and (l) degree of pain sensitivity for different gate–channel combinations. Reprinted with permission from [153]. Copyright 2009, Royal Society of Chemistry.

Fu et al. proposed a kind of charge-regulated FET (CRFET) to realize an artificial pain-perceptual system that adopted graphene as a channel and Gd_xO_y/Al_xO_y as dielectric

layers to provide opposite polarities of oxide charges [152]. The Gd_xO_y dielectric layer containing positive oxide charges plays an important role in the IPSC/EPSC behaviors. However, the neuromorphic behaviors would be opposite for the Al_xO_y dielectric layer with negative oxide charges. An artificial pain modulation system (PMS) was proposed based on the above behaviors [152]. Figure 7g shows biological PMS and artificial PMS. The enhanced conductivity of the memristor can increase the voltage drop of the channel and effectively suppress the amplitude of the signal from the gate, as shown in Figure 7h. Figure 7i shows the ability of the pre-synapse to inhibit both pre- and post-stimulus signals.

For array networks, Li et al. utilized sodium alginate (SA) as a common neurotransmitter layer to fabricate a 5×5 ionotronic junctionless indium-tin-oxide transistor array for realizing pain-perception and threshold-modulation functions [153]. Figure 7j shows the oxide transistor array and test system. Pain is also recognized by defining a threshold current, as shown in Figure 7k,l. A coplanar-multiterminal transistor array is very suitable for not only realizing the nociceptor networks but also avoiding complex architectures with multiple layers, interconnects, or other complex components. Moreover, this particular structure also has the ability to modulate synaptic weights according to spatial orientation, through which orientation-dependent spike timing plasticity learning rules can be successfully implemented. Such devices provide a viable method for building spatiotemporally correlated neuromorphic systems [154]. This device can provide a novel approach for achieving praiseworthy pain-perceptual functions and may also create a new opportunity for oxide transistor arrays in future multifunctional robotics and auxiliary equipment.

5. Conclusions and Perspectives

This review investigates neuromorphic devices based on metal-oxide heterostructures, encompassing their fabrication, properties, and applications. Initially, we discuss various preparation methodologies for metal oxides, including both bottom-up and top-down approaches. Subsequently, the fabrication methods and properties of metal-oxide heterostructures are elaborated. Further, the review delves into different neuromorphic device architectures with metal-oxide heterostructures, including two-terminal memristors as well as three-terminal transistors. More importantly, we present the recent progress in their neuromorphic applications, including in visual, tactile, and nociceptive systems. Metal-oxide heterostructures have several advantages, such as low power consumption, high stability, and excellent electrical performance. However, there are still several challenges that cannot be overlooked. Due to the nonlinear and dynamic nature of metal-oxide heterostructures, there are various aspects that need to be considered when constructing metal-oxide heterostructures, such as determining how to obtain a combination of the excellent properties of the two materials and make them outstanding while at the same time keeping other poor properties of the two materials that are not conducive to the performance of the device from becoming outstanding. The integration of metal-oxide-based neuromorphic devices with existing silicon-based electronic devices still faces compatibility and interconnectivity challenges, as the fabrication of metal-oxide heterostructures is incompatible with conventional CMOS fabrication techniques. As far as bionic sensing systems are concerned, most of the current research has only been directed towards systems with a single sensing capability through the integration of sensors and synaptic devices, e.g., vision and haptics.

In light of these drawbacks, several remedial strategies can be considered. Firstly, data analytics based on a machine learning approach could be employed to accurately predict material properties and device performance. Secondly, researchers could investigate metal-oxide materials and device structures that are compatible with existing CMOS processes. Also, researchers could develop simplified manufacturing processes to reduce manufacturing steps and costs. Then, they could design flexible interface technologies for the seamless integration of metal-oxide devices with silicon-based circuits. Also, they could develop modular designs so that components from different technologies can be easily integrated. Finally, new micro- and nanofabrication techniques for reducing device variability and leakage on small scales should be researched and developed. Also, 3D

integration techniques for increasing device density without sacrificing performance should be explored.

Nevertheless, neuromorphic devices based on metal-oxide heterojunctions integrating sensing, storage, and computing are urgently needed for the booming fields of artificial intelligence and machine learning. Therefore, research on synaptic devices based on metal-oxide heterojunctions is an exciting topic in the age of intelligence. From the perspective of future applications, especially in the field of self-driving cars, smart sensors, and personalized medicine, the functions of metal-oxide heterojunction neuromorphic devices in synapse emulation, image sensing, and preprocessing will be further developed through rational material selection and device structure design. In conclusion, the field of metal-oxide heterostructures for neuromorphic applications holds great promise for revolutionizing various aspects of computing and artificial intelligence. Continued research and development in this area are expected to yield groundbreaking advancements in the coming years.

Funding: This work was supported by Hunan Science Fund for Distinguished Young Scholars (2023JJ10069) and the National Natural Science Foundation of China (52172169).

Conflicts of Interest: The authors declare no conflict of interest.

References

1. Marjani, M.; Nasaruddin, F.; Gani, A.; Karim, A.; Hashem, I.A.T.; Siddiq, A.; Yaqoob, I. Big IoT Data Analytics: Architecture, Opportunities, and Open Research Challenges. *IEEE Access* **2017**, *5*, 5247–5261. [[CrossRef](#)]
2. Gibney, E. Google AI Algorithm Masters Ancient Game of Go. *Nature* **2016**, *529*, 445–446. [[CrossRef](#)]
3. Yu, S. Neuro-Inspired Computing with Emerging Nonvolatile Memorys. *Proc. IEEE* **2018**, *106*, 260–285. [[CrossRef](#)]
4. Neumann, J. von First Draft of a Report on the EDVAC. *IEEE Ann. Hist. Comput.* **1993**, *15*, 27–75. [[CrossRef](#)]
5. Najafabadi, M.M.; Villanustre, F.; Khoshgoftaar, T.M.; Seliya, N.; Wald, R.; Muharemagic, E. Deep Learning Applications and Challenges in Big Data Analytics. *J. Big Data* **2015**, *2*, 1. [[CrossRef](#)]
6. Wu, Y.; Feng, J. Development and Application of Artificial Neural Network. *Wirel. Pers. Commun.* **2018**, *102*, 1645–1656. [[CrossRef](#)]
7. Moore, G.E. Cramming More Components onto Integrated Circuits, Reprinted from Electronics, Volume 38, Number 8, April 19, 1965, pp.114 ff. *IEEE Solid-State Circuits Soc. Newsl.* **2006**, *11*, 33–35. [[CrossRef](#)]
8. Kandel, E.R.; Koester, J.D.; Mack, S.H.; Siegelbaum, S.A. *Principles of Neural Science*, 6th ed.; McGraw Hill: New York, NY, USA, 2021.
9. Oh, C.; Jo, M.; Son, J. All-Solid-State Synaptic Transistors with High-Temperature Stability Using Proton Pump Gating of Strongly Correlated Materials. *ACS Appl. Mater. Interfaces* **2019**, *11*, 15733–15740. [[CrossRef](#)]
10. He, Y.; Yang, Y.; Nie, S.; Liu, R.; Wan, Q. Electric-Double-Layer Transistors for Synaptic Devices and Neuromorphic Systems. *J. Mater. Chem. C* **2018**, *6*, 5336–5352. [[CrossRef](#)]
11. Merolla, P.A.; Arthur, J.V.; Alvarez-Icaza, R.; Cassidy, A.S.; Sawada, J.; Akopyan, F.; Jackson, B.L.; Imam, N.; Guo, C.; Nakamura, Y.; et al. A Million Spiking-Neuron Integrated Circuit with a Scalable Communication Network and Interface. *Science* **2014**, *345*, 668–673. [[CrossRef](#)]
12. Kim, Y.-H.; Heo, J.-S.; Kim, T.-H.; Park, S.; Yoon, M.-H.; Kim, J.; Oh, M.S.; Yi, G.-R.; Noh, Y.-Y.; Park, S.K. Flexible Metal-Oxide Devices Made by Room-Temperature Photochemical Activation of Sol–Gel Films. *Nature* **2012**, *489*, 128–132. [[CrossRef](#)] [[PubMed](#)]
13. Banger, K.K.; Yamashita, Y.; Mori, K.; Peterson, R.L.; Leedham, T.; Rickard, J.; Sirringhaus, H. Low-Temperature, High-Performance Solution-Processed Metal Oxide Thin-Film Transistors Formed by a ‘Sol–Gel on Chip’ Process. *Nat. Mater.* **2011**, *10*, 45–50. [[CrossRef](#)] [[PubMed](#)]
14. Yu, X.; Marks, T.J.; Facchetti, A. Metal Oxides for Optoelectronic Applications. *Nat. Mater.* **2016**, *15*, 383–396. [[CrossRef](#)]
15. Gai, L.-Y.; Lai, R.-P.; Dong, X.-H.; Wu, X.; Luan, Q.-T.; Wang, J.; Lin, H.-F.; Ding, W.-H.; Wu, G.-L.; Xie, W.-F. Recent Advances in Ethanol Gas Sensors Based on Metal Oxide Semiconductor Heterojunctions. *Rare Met.* **2022**, *41*, 1818–1842. [[CrossRef](#)]
16. Yao, Y.; Sang, D.; Duan, S.; Wang, Q.; Liu, C. Review on the Properties of Boron-Doped Diamond and One-Dimensional-Metal-Oxide Based P-N Heterojunction. *Molecules* **2021**, *26*, 71. [[CrossRef](#)] [[PubMed](#)]
17. Zhang, N.; Jiang, R. Interfacial Engineering of Metal/Metal Oxide Heterojunctions toward Oxygen Reduction and Evolution Reactions. *ChemPlusChem* **2021**, *86*, 1586–1601. [[CrossRef](#)]
18. Li, T.; Zeng, W.; Wang, Z. Quasi-One-Dimensional Metal-Oxide-Based Heterostructural Gas-Sensing Materials: A Review. *Sens. Actuators B Chem.* **2015**, *221*, 1570–1585. [[CrossRef](#)]
19. Du, P.-F.; Feng, P.; Wan, X.; Yang, Y.; Wan, Q. Amorphous InGaZnO₄ Neuron Transistors with Temporal and Spatial Summation Function. *Chin. Phys. Lett.* **2017**, *34*, 058502. [[CrossRef](#)]
20. Zhu, Y.; He, Y.; Jiang, S.; Zhu, L.; Chen, C.; Wan, Q. Indium–Gallium–Zinc–Oxide Thin-Film Transistors: Materials, Devices, and Applications. *J. Semicond.* **2021**, *42*, 031101. [[CrossRef](#)]

21. Guo, T.; Sun, B.; Ranjan, S.; Jiao, Y.; Wei, L.; Zhou, Y.N.; Wu, Y.A. From Memristive Materials to Neural Networks. *ACS Appl. Mater. Interfaces* **2020**, *12*, 54243–54265. [[CrossRef](#)]
22. Pasquarelli, R.; Ginley, D.; O'Hayre, R. ChemInform Abstract: Solution Processing of Transparent Conductors: From Flask to Film. *Chem. Soc. Rev.* **2011**, *40*, 5406–5441. [[CrossRef](#)] [[PubMed](#)]
23. Zakaria, S.N.F.; Aziz, H.A.; Hung, Y.-T.; Mojiri, A.; Glysson, E.A. Mechanical Volume Reduction. In *Solid Waste Engineering and Management: Volume 1*; Wang, L.K., Wang, M.-H.S., Hung, Y.-T., Eds.; Springer International Publishing: Cham, Switzerland, 2021; pp. 297–343. ISBN 978-3-030-84180-5.
24. Chen, Y.; Gao, G.; Zhao, J.; Zhang, H.; Yu, J.; Yang, X.; Zhang, Q.; Zhang, W.; Xu, S.; Sun, J.; et al. Piezotronic Graphene Artificial Sensory Synapse. *Adv. Funct. Mater.* **2019**, *29*, 1900959. [[CrossRef](#)]
25. Feng, G.; Jiang, J.; Zhao, Y.; Wang, S.; Liu, B.; Yin, K.; Niu, D.; Li, X.; Chen, Y.; Duan, H.; et al. A Sub-10 Nm Vertical Organic/Inorganic Hybrid Transistor for Pain-Perceptual and Sensitization-Regulated Nociceptor Emulation. *Adv. Mater.* **2020**, *32*, 1906171. [[CrossRef](#)] [[PubMed](#)]
26. Xie, D.; Wei, L.; Xie, M.; Jiang, L.; Yang, J.; He, J.; Jiang, J. Photoelectric Visual Adaptation Based on 0D-CsPbBr₃-Quantum-Dots/2D-MoS₂ Mixed-Dimensional Heterojunction Transistor. *Adv. Funct. Mater.* **2021**, *31*, 2010655. [[CrossRef](#)]
27. Liang, K.; Wang, R.; Huo, B.; Ren, H.; Li, D.; Wang, Y.; Tang, Y.; Chen, Y.; Song, C.; Li, F.; et al. Fully Printed Optoelectronic Synaptic Transistors Based on Quantum Dot–Metal Oxide Semiconductor Heterojunctions. *ACS Nano* **2022**, *16*, 8651–8661. [[CrossRef](#)]
28. Sakka, S.; Kozuka, H.; Zhao, G. Sol-Gel Preparation of Metal Particle/Oxide Nanocomposites. In *Proceedings of the Sol-Gel Optics III*; SPIE: Bellingham, WA, USA, 1994; Volume 2288, pp. 108–119.
29. Ou, N.C.; Su, X.; Bock, D.C.; McElwee-White, L. Precursors for Chemical Vapor Deposition of Tungsten Oxide and Molybdenum Oxide. *Coord. Chem. Rev.* **2020**, *421*, 213459. [[CrossRef](#)]
30. Zhao, Q.; Zhao, D.; Zhao, J.; Fei, L. The Song Dynasty Shipwreck Monitoring and Analysis Using Acoustic Emission Technique. *Forests* **2019**, *10*, 767. [[CrossRef](#)]
31. Malandrino, G. Chemical Vapour Deposition. Precursors, Processes and Applications. *Angew. Chem. Int. Ed.* **2009**, *48*, 7478–7479. [[CrossRef](#)]
32. Yin, T.-H.; Liu, B.-J.; Lin, Y.-W.; Li, Y.-S.; Lai, C.-W.; Lan, Y.-P.; Choi, C.; Chang, H.-C.; Choi, Y. Electrodeposition of Copper Oxides as Cost-Effective Heterojunction Photoelectrode Materials for Solar Water Splitting. *Coatings* **2022**, *12*, 1839. [[CrossRef](#)]
33. Hu, R.; Liao, Y.; Qiao, H.; Li, J.; Wang, K.; Huang, Z.; Qi, X. Electrochemical Method Integrating Exfoliation and In-Situ Growth to Synthesize MoS₂ Nanosheets/MnO₂ Heterojunction for Performance-Enhanced Supercapacitor. *Ceram. Int.* **2022**, *48*, 23498–23503. [[CrossRef](#)]
34. Pedersen, J.D.; Esposito, H.J.; Teh, K.S. Direct Synthesis and Characterization of Optically Transparent Conformal Zinc Oxide Nanocrystalline Thin Films by Rapid Thermal Plasma CVD. *Nanoscale Res. Lett.* **2011**, *6*, 568. [[CrossRef](#)]
35. Kumeria, T.; Santos, A.; Losic, D. Nanoporous Anodic Alumina Platforms: Engineered Surface Chemistry and Structure for Optical Sensing Applications. *Sensors* **2014**, *14*, 11878–11918. [[CrossRef](#)]
36. Reports, W.M. Physical Vapor Deposition Market Will Reach New Heights in the Upcoming Year 2022–2029. Oerlikon Balzers (Oerlikon Group), IHI Corporation, Silfex Inc. (Lam Research Corp.). Available online: <https://www.openpr.com/news/2741878/physical-vapor-deposition-market-will-reach-new-heights-in> (accessed on 27 October 2023).
37. Roostaei, T.; Rahimpour, M.R.; Zhao, H.; Eisapour, M.; Chen, Z.; Hu, J. Recent Advances and Progress in Biotemplate Catalysts for Electrochemical Energy Storage and Conversion. *Adv. Colloid Interface Sci.* **2023**, *318*, 102958. [[CrossRef](#)]
38. Ito, M.; Furumoto, D. Effects of Mechanical Milling and Ag Addition on Thermoelectric Properties of Na_xCo₂O₄. *Scr. Mater.* **2006**, *55*, 533–536. [[CrossRef](#)]
39. Campbell, S.A. *The Science and Engineering of Microelectronic Fabrication*; Oxford University Press: New York, NY, USA, 2001; ISBN 978-0-19-513605-0.
40. O'Sullivan, J.; Burgess, S.; Rimmer, N. Metal Lift-off Using Physical Vapour Deposition. *Microelectron. Eng.* **2002**, *64*, 473–478. [[CrossRef](#)]
41. Radulescu, F.; Miller, P.; Cunnane, L.; Harris, M.; Lam, H.; Bowers, C. Complete Sputtering Metallization for High-Volume Manufacturing. *III-Vs Rev.* **2002**, *15*, 42–45. [[CrossRef](#)]
42. Wong, Y.H.; Cheong, K.Y. ZrO₂ Thin Films on Si Substrate. *J. Mater. Sci. Mater. Electron.* **2010**, *21*, 980–993. [[CrossRef](#)]
43. Chin, W.C.; Cheong, K.Y.; Hassan, Z. Sm₂O₃ Gate Dielectric on Si Substrate. *Mater. Sci. Semicond. Process.* **2010**, *13*, 303–314. [[CrossRef](#)]
44. Nakazawa, H.; Sudoh, A.; Suemitsu, M.; Yasui, K.; Itoh, T.; Endoh, T.; Narita, Y.; Mashita, M. Mechanical and Tribological Properties of Boron, Nitrogen-Coincorporated Diamond-like Carbon Films Prepared by Reactive Radio-Frequency Magnetron Sputtering. *Diam. Relat. Mater.* **2010**, *19*, 503–506. [[CrossRef](#)]
45. Wasa, K.; Kitabatake, M.; Adachi, H. 4—Sputtering Systems. In *Thin Film Materials Technology*; Wasa, K., Kitabatake, M., Adachi, H., Eds.; William Andrew Publishing: Norwich, NY, USA, 2004; pp. 115–189. ISBN 978-0-8155-1483-1.
46. Wasa, K.; Kitabatake, M.; Adachi, H. 5—Deposition of Compound Thin Films. In *Thin Film Materials Technology*; Wasa, K., Kitabatake, M., Adachi, H., Eds.; William Andrew Publishing: Norwich, NY, USA, 2004; pp. 191–403. ISBN 978-0-8155-1483-1.

47. Wasa, K.; Kitabatake, M.; Adachi, H. 6—Structural Control of Compound Thin Films: Perovskite and Nanometer Oxide Thin Films. In *Thin Film Materials Technology*; Wasa, K., Kitabatake, M., Adachi, H., Eds.; William Andrew Publishing: Norwich, NY, USA, 2004; pp. 405–463. ISBN 978-0-8155-1483-1.
48. Ni, Y.; Liu, L.; Liu, J.; Xu, W. A High-Strength Neuromuscular System That Implements Reflexes as Controlled by a Multiquadrant Artificial Efferent Nerve. *ACS Nano* **2022**, *16*, 20294–20304. [[CrossRef](#)]
49. Sassella, A.; Campione, M.; Raimondo, L.; Tavazzi, S.; Borghesi, A.; Goletti, C.; Bussetti, G.; Chiaradia, P. Epitaxial Growth of Organic Heterostructures: Morphology, Structure, and Growth Mode. *Surf. Sci.* **2007**, *601*, 2571–2575. [[CrossRef](#)]
50. Zhang, Y.; Gao, Y.; Carvalho, W.S.P.; Fang, C.; Serpe, M.J. Microgel-Based Stretchable Reservoir Devices for Elongation Enhanced Small Molecule Release Rate. *ACS Appl. Mater. Interfaces* **2020**, *12*, 19062–19068. [[CrossRef](#)]
51. Harhouz, A.; Hocini, A.; Tayoub, H. Ultracompact Gas-Sensor Based on a 2D Photonic Crystal Waveguide Incorporating with Tapered Microcavity. *IOP Conf. Ser. Mater. Sci. Eng.* **2021**, *1046*, 012001. [[CrossRef](#)]
52. Liu, Z.; Li, M.; Sun, Y.; Wang, H.; Chen, H.; Tian, Y.; Wang, H.; Ding, Y.; Chen, Z. Integrating Surface and Interface Engineering to Improve Optoelectronic Performance and Environmental Stability of MXene-Based Heterojunction towards Broadband Photodetection. *Nano Res.* **2023**, *16*, 10148–10155. [[CrossRef](#)]
53. Shen, R.; Jiang, C.; Xiang, Q.; Xie, J.; Li, X. Surface and Interface Engineering of Hierarchical Photocatalysts. *Appl. Surf. Sci.* **2019**, *471*, 43–87. [[CrossRef](#)]
54. Koretomo, D.; Hamada, S.; Magari, Y.; Furuta, M. Quantum Confinement Effect in Amorphous In–Ga–Zn–O Heterojunction Channels for Thin-Film Transistors. *Materials* **2020**, *13*, 1935. [[CrossRef](#)]
55. Shi, J.; Starr, M.B.; Wang, X. Band Structure Engineering at Heterojunction Interfaces via the Piezotronic Effect. *Adv. Mater.* **2012**, *24*, 4683–4691. [[CrossRef](#)]
56. Lu, L.; Xu, T.; Chen, W.; Lee, J.M.; Luo, Z.; Jung, I.H.; Park, H.I.; Kim, S.O.; Yu, L. The Role of N-Doped Multiwall Carbon Nanotubes in Achieving Highly Efficient Polymer Bulk Heterojunction Solar Cells. *Nano Lett.* **2013**, *13*, 2365–2369. [[CrossRef](#)]
57. Lemmermann, T.; Becker, M.; Stehle, M.; Drache, M.; Beuermann, S.; Bogar, M.S.; Gohs, U.; Fittschen, U.E.A.; Turek, T.; Kunz, U. In Situ and in Operando Detection of Redox Reactions with Integrated Potential Probes during Vanadium Transport in Ion Exchange Membranes. *J. Power Source* **2022**, *533*, 231343. [[CrossRef](#)]
58. Ge, Y.; Liu, Z.; Wu, Y.; Holze, R. On the Utilization of Supercapacitor Electrode Materials. *Electrochim. Acta* **2021**, *366*, 137390. [[CrossRef](#)]
59. Lu, W.; Shen, J.; Zhang, P.; Zhong, Y.; Hu, Y.; Lou, X.W. Construction of CoO/Co-Cu-S Hierarchical Tubular Heterostructures for Hybrid Supercapacitors. *Angew. Chem.* **2019**, *131*, 15587–15593. [[CrossRef](#)]
60. Zhang, Y.; Huang, L.; Lei, X.; Huang, H.; Guo, W.; Wang, S. Hierarchical Ternary Zn-Ni-Co Sulfide/Oxide Heterostructure for High Specific Energy Hybrid Supercapacitor. *J. Alloys Compd.* **2023**, *962*, 171201. [[CrossRef](#)]
61. Ju, H.; Tang, Q.; Xu, Y.; Bai, X.; Pu, C.; Liu, T.; Liu, S.; Zhang, L. Prussian Blue Analogue-Derived Hollow Metal Oxide Heterostructure for High-Performance Supercapacitors. *Dalton Trans.* **2023**, *52*, 12948–12957. [[CrossRef](#)] [[PubMed](#)]
62. Ye, R.; Zhu, J.; Tong, Y.; Feng, D.; Chen, P. Metal Oxides Heterojunction Derived Bi-In Hybrid Electrocatalyst for Robust Electroreduction of CO₂ to Formate. *J. Energy Chem.* **2023**, *83*, 180–188. [[CrossRef](#)]
63. Rajak, R.; Saraf, M.; Mobin, S.M. Robust Heterostructures of a Bimetallic Sodium–Zinc Metal–Organic Framework and Reduced Graphene Oxide for High-Performance Supercapacitors. *J. Mater. Chem. A* **2019**, *7*, 1725–1736. [[CrossRef](#)]
64. Zhang, Y.; Li, L.; Su, H.; Huang, W.; Dong, X. Binary Metal Oxide: Advanced Energy Storage Materials in Supercapacitors. *J. Mater. Chem. A* **2015**, *3*, 43–59. [[CrossRef](#)]
65. Jia, J.; Hao, X.; Chang, Y.; Jia, M.; Wen, Z. Rational Design of Cu₃PdN Nanocrystals for Selective Electroreduction of Carbon Dioxide to Formic Acid. *J. Colloid Interface Sci.* **2021**, *586*, 491–497. [[CrossRef](#)]
66. Zhu, W.; Zhao, K.; Liu, S.; Liu, M.; Peng, F.; An, P.; Qin, B.; Zhou, H.; Li, H.; He, Z. Low-Overpotential Selective Reduction of CO₂ to Ethanol on Electrodeposited CuxAuy Nanowire Arrays. *J. Energy Chem.* **2019**, *37*, 176–182. [[CrossRef](#)]
67. Dai, W.; Long, J.; Yang, L.; Zhang, S.; Xu, Y.; Luo, X.; Zou, J.; Luo, S. Oxygen Migration Triggering Molybdenum Exposure in Oxygen Vacancy-Rich Ultra-Thin Bi₂MoO₆ Nanoflakes: Dual Binding Sites Governing Selective CO₂ Reduction into Liquid Hydrocarbons. *J. Energy Chem.* **2021**, *61*, 281–289. [[CrossRef](#)]
68. Wang, S.; Kou, T.; Baker, S.E.; Duoss, E.B.; Li, Y. Recent Progress in Electrochemical Reduction of CO₂ by Oxide-Derived Copper Catalysts. *Mater. Today Nano* **2020**, *12*, 100096. [[CrossRef](#)]
69. Li, F.; Chen, L.; Xue, M.; Williams, T.; Zhang, Y.; MacFarlane, D.R.; Zhang, J. Towards a Better Sn: Efficient Electrocatalytic Reduction of CO₂ to Formate by Sn/SnS₂ Derived from SnS₂ Nanosheets. *Nano Energy* **2017**, *31*, 270–277. [[CrossRef](#)]
70. Tan, D.; Lee, W.; Kim, Y.E.; Ko, Y.N.; Youn, M.H.; Jeon, Y.E.; Hong, J.; Park, J.E.; Seo, J.; Jeong, S.K.; et al. In–Bi Electrocatalyst for the Reduction of CO₂ to Formate in a Wide Potential Window. *ACS Appl. Mater. Interfaces* **2022**, *14*, 28890–28899. [[CrossRef](#)] [[PubMed](#)]
71. Wu, M.; Xiong, Y.; Hu, B.; Zhang, Z.; Wei, B.; Li, L.; Hao, J.; Shi, W. Indium Doped Bismuth Subcarbonate Nanosheets for Efficient Electrochemical Reduction of Carbon Dioxide to Formate in a Wide Potential Window. *J. Colloid Interface Sci.* **2022**, *624*, 261–269. [[CrossRef](#)]
72. Wang, Q.; Yang, X.; Zang, H.; Chen, F.; Wang, C.; Yu, N.; Geng, B. Metal–Organic Framework-Derived BiIn Bimetallic Oxide Nanoparticles Embedded in Carbon Networks for Efficient Electrochemical Reduction of CO₂ to Formate. *Inorg. Chem.* **2022**, *61*, 12003–12011. [[CrossRef](#)]

73. Purves, D.; Augustine, G.J.; Fitzpatrick, D.; Hall, W.; LaMantia, A.-S.; White, L. *Neurosciences*; De Boeck Supérieur: Paris, France, 2019; ISBN 2-8073-1492-9.
74. Pakkenberg, B.; Pelvig, D.; Marner, L.; Bundgaard, M.J.; Gundersen, H.J.G.; Nyengaard, J.R.; Regeur, L. Aging and the Human Neocortex. *Exp. Gerontol.* **2003**, *38*, 95–99. [[CrossRef](#)] [[PubMed](#)]
75. Goto, A. Synaptic Plasticity during Systems Memory Consolidation. *Neurosci. Res.* **2022**, *183*, 1–6. [[CrossRef](#)] [[PubMed](#)]
76. Trepel, C.; Racine, R.J. Long-Term Potentiation in the Neocortex of the Adult, Freely Moving Rat. *Cereb. Cortex* **1998**, *8*, 719–729. [[CrossRef](#)]
77. Remondina, J.; Golubev, N.V.; Ignat'eva, E.S.; Sigaev, V.N.; Acciarri, M.; Paleari, A.; Lorenzi, R. Random Networks of Disconnected Nanoparticles in Dielectric Layers as a Source of Electric Responsivity. *Mater. Des.* **2023**, *228*, 111825. [[CrossRef](#)]
78. Luo, L. *Principles of Neurobiology*; Garland Science, Taylor & Francis Group, LLC: New York, NY, USA, 2016.
79. Liu, Q.; Yin, L.; Zhao, C.; Wu, Z.; Wang, J.; Yu, X.; Wang, Z.; Wei, W.; Liu, Y.; Mitrovic, I.Z.; et al. All-in-One Metal-Oxide Heterojunction Artificial Synapses for Visual Sensory and Neuromorphic Computing Systems. *Nano Energy* **2022**, *97*, 107171. [[CrossRef](#)]
80. Li, J.; Jiang, D.; Yang, Y.; Zhou, Y.; Chen, Q.; Zhang, J. Li-Ion Doping as a Strategy to Modulate the Electrical-Double-Layer for Improved Memory and Learning Behavior of Synapse Transistor Based on Fully Aqueous-Solution-Processed In₂O₃/AlLiO Film. *Adv. Electron. Mater.* **2020**, *6*, 1901363. [[CrossRef](#)]
81. Zhu, Y.; Liu, G.; Xin, Z.; Fu, C.; Wan, Q.; Shan, F. Solution-Processed, Electrolyte-Gated In₂O₃ Flexible Synaptic Transistors for Brain-Inspired Neuromorphic Applications. *ACS Appl. Mater. Interfaces* **2020**, *12*, 1061–1068. [[CrossRef](#)] [[PubMed](#)]
82. Rolls, E.T.; Dempere-Marco, L.; Deco, G. Holding Multiple Items in Short Term Memory: A Neural Mechanism. *PLoS ONE* **2013**, *8*, e61078. [[CrossRef](#)]
83. Lynch, M.A. Long-Term Potentiation and Memory. *Physiol. Rev.* **2004**, *84*, 87–136. [[CrossRef](#)]
84. Sawa, A. Resistive Switching in Transition Metal Oxides. *Mater. Today* **2008**, *11*, 28–36. [[CrossRef](#)]
85. Waser, R.; Aono, M. Nanoionics-Based Resistive Switching Memories. *Nat. Mater.* **2007**, *6*, 833–840. [[CrossRef](#)]
86. Gao, B.; Sun, B.; Zhang, H.; Liu, L.; Liu, X.; Han, R.; Kang, J.; Yu, B. Unified Physical Model of Bipolar Oxide-Based Resistive Switching Memory. *IEEE Electron Device Lett.* **2009**, *30*, 1326–1328. [[CrossRef](#)]
87. Waser, R.; Dittmann, R.; Staikov, G.; Szot, K. Redox-Based Resistive Switching Memories—Nanoionic Mechanisms, Prospects, and Challenges. *Adv. Mater.* **2009**, *21*, 2632–2663. [[CrossRef](#)] [[PubMed](#)]
88. Gao, B.; Kang, J.F.; Chen, Y.S.; Zhang, F.F.; Chen, B.; Huang, P.; Liu, L.F.; Liu, X.Y.; Wang, Y.Y.; Tran, X.A.; et al. Oxide-Based RRAM: Unified Microscopic Principle for Both Unipolar and Bipolar Switching. In Proceedings of the 2011 International Electron Devices Meeting, Washington, DC, USA, 5–7 December 2011; pp. 17.4.1–17.4.4.
89. Wang, Z.; Yin, M.; Zhang, T.; Cai, Y.; Wang, Y.; Yang, Y.; Huang, R. Engineering Incremental Resistive Switching in TaOx Based Memristors for Brain-Inspired Computing. *Nanoscale* **2016**, *8*, 14015–14022. [[CrossRef](#)]
90. Kim, S.G.; Han, J.S.; Kim, H.; Kim, S.Y.; Jang, H.W. Recent Advances in Memristive Materials for Artificial Synapses. *Adv. Mater. Technol.* **2018**, *3*, 1800457. [[CrossRef](#)]
91. Pickett, M.D.; Strukov, D.B.; Borghetti, J.L.; Yang, J.J.; Snider, G.S.; Stewart, D.R.; Williams, R.S. Switching Dynamics in Titanium Dioxide Memristive Devices. *J. Appl. Phys.* **2009**, *106*, 074508. [[CrossRef](#)]
92. Hansen, M.; Ziegler, M.; Kolberg, L.; Soni, R.; Dirkmann, S.; Mussenbrock, T.; Kohlstedt, H. A Double Barrier Memristive Device. *Sci. Rep.* **2015**, *5*, 13753. [[CrossRef](#)]
93. Wu, Q.; Wang, J.; Cao, J.; Lu, C.; Yang, G.; Shi, X.; Chuai, X.; Gong, Y.; Su, Y.; Zhao, Y.; et al. Photoelectric Plasticity in Oxide Thin Film Transistors with Tunable Synaptic Functions. *Adv. Electron. Mater.* **2018**, *4*, 1800556. [[CrossRef](#)]
94. Zhou, Y.; Li, J.; Yang, Y.; Chen, Q.; Zhang, J. Artificial Synapse Emulated through Fully Aqueous Solution-Processed Low-Voltage In₂O₃ Thin-Film Transistor with Gd₂O₃ Solid Electrolyte. *ACS Appl. Mater. Interfaces* **2020**, *12*, 980–988. [[CrossRef](#)] [[PubMed](#)]
95. Dai, C.; Huo, C.; Qi, S.; Dai, M.; Webster, T.; Xiao, H. Flexible and Transparent Artificial Synapse Devices Based on Thin-Film Transistors with Nanometer Thickness. *Int. J. Nanomed.* **2020**, *15*, 8037–8043. [[CrossRef](#)] [[PubMed](#)]
96. Beom, K.; Han, J.; Kim, H.-M.; Yoon, T.-S. Wide Range Modulation of Synaptic Weight in Thin-Film Transistors with Hafnium Oxide Gate Insulator and Indium-Zinc Oxide Channel Layer for Artificial Synapse Application. *Nanoscale* **2021**, *13*, 11370–11379. [[CrossRef](#)] [[PubMed](#)]
97. Khan, M.A.; Yim, S.; Rehman, S.; Ghafoor, F.; Kim, H.; Patil, H.; Khan, M.F.; Eom, J. Two-Dimensional Materials Memory Devices with Floating Metal Gate for Neuromorphic Applications. *Mater. Today Adv.* **2023**, *20*, 100438. [[CrossRef](#)]
98. Morosawa, N.; Nishiyama, M.; Ohshima, Y.; Sato, A.; Terai, Y.; Tokunaga, K.; Iwasaki, J.; Akamatsu, K.; Kanitani, Y.; Tanaka, S.; et al. High-Mobility Self-Aligned Top-Gate Oxide TFT for High-Resolution AM-OLED: High-Mobility Self-Aligned Top-Gate Oxide TFT. *J. Soc. Inf. Disp.* **2013**, *21*, 467–473. [[CrossRef](#)]
99. Allendorf, M.D.; Dong, R.; Feng, X.; Kaskel, S.; Matoga, D.; Stavila, V. Electronic Devices Using Open Framework Materials. *Chem. Rev.* **2020**, *120*, 8581–8640. [[CrossRef](#)]
100. Rehman, S.; Khan, M.F.; Rahmani, M.K.; Kim, H.; Patil, H.; Khan, S.A.; Kang, M.H.; Kim, D. Neuro-Transistor Based on UV-Treated Charge Trapping in MoTe₂ for Artificial Synaptic Features. *Nanomaterials* **2020**, *10*, 2326. [[CrossRef](#)]
101. Weimer, P.K. The TFT A New Thin-Film Transistor. *Proc. IRE* **1962**, *50*, 1462–1469. [[CrossRef](#)]
102. Kuo, Y. Thin Film Transistor Technology—Past, Present, and Future. *Electrochem. Soc. Interface* **2013**, *22*, 55. [[CrossRef](#)]
103. Klasens, H.A.; Koelmans, H. A Tin Oxide Field-Effect Transistor. *Solid-State Electron.* **1964**, *7*, 701–702. [[CrossRef](#)]

104. Nomura, K.; Ohta, H.; Takagi, A.; Kamiya, T.; Hirano, M.; Hosono, H. Room-Temperature Fabrication of Transparent Flexible Thin-Film Transistors Using Amorphous Oxide Semiconductors. *Nature* **2004**, *432*, 488–492. [[CrossRef](#)] [[PubMed](#)]
105. Rim, Y.S. Review of Metal Oxide Semiconductors-Based Thin-Film Transistors for Point-of-Care Sensor Applications. *J. Inf. Disp.* **2020**, *21*, 203–210. [[CrossRef](#)]
106. Mirshojaeian Hosseini, M.J.; Nawrocki, R.A. A Review of the Progress of Thin-Film Transistors and Their Technologies for Flexible Electronics. *Micromachines* **2021**, *12*, 655. [[CrossRef](#)] [[PubMed](#)]
107. Duan, N.; Li, Y.; Chiang, H.-C.; Chen, J.; Pan, W.-Q.; Zhou, Y.-X.; Chien, Y.-C.; He, Y.-H.; Xue, K.-H.; Liu, G.; et al. An Electro-Photo-Sensitive Synaptic Transistor for Edge Neuromorphic Visual Systems. *Nanoscale* **2019**, *11*, 17590–17599. [[CrossRef](#)] [[PubMed](#)]
108. Wang, J.; Liu, S. Visual Information Computing and Processing Model Based on Artificial Neural Network. *Comput. Intell. Neurosci.* **2022**, *2022*, 4713311. [[CrossRef](#)] [[PubMed](#)]
109. Meng, J.; Wang, T.; Zhu, H.; Ji, L.; Bao, W.; Zhou, P.; Chen, L.; Sun, Q.-Q.; Zhang, D.W. Integrated In-Sensor Computing Optoelectronic Device for Environment-Adaptable Artificial Retina Perception Application. *Nano Lett.* **2022**, *22*, 81–89. [[CrossRef](#)]
110. Jiang, Z.; Jiang, Y.; Chen, N.; Chen, X. Artificial Visual Electronics for Closed-Loop Sensation/Action Systems. *Adv. Intell. Syst.* **2021**, *3*, 2100071. [[CrossRef](#)]
111. Pei, Y.; Yan, L.; Wu, Z.; Lu, J.; Zhao, J.; Chen, J.; Liu, Q.; Yan, X. Artificial Visual Perception Nervous System Based on Low-Dimensional Material Photoelectric Memristors. *ACS Nano* **2021**, *15*, 17319–17326. [[CrossRef](#)]
112. Hong, S.; Cho, H.; Kang, B.H.; Park, K.; Akinwande, D.; Kim, H.J.; Kim, S. Neuromorphic Active Pixel Image Sensor Array for Visual Memory. *ACS Nano* **2021**, *15*, 15362–15370. [[CrossRef](#)]
113. Yang, J.S.; Jung, S.H.; Kim, D.S.; Choi, J.H.; Suh, H.W.; Lee, H.H.; Lee, K.W.; Cho, H.K. Design of Functionally Stacked Channels of Oxide Thin-Film Transistors to Mimic Precise Ultralow-Light-Irradiated Synaptic Weight Modulation. *Micromachines* **2022**, *13*, 526. [[CrossRef](#)]
114. Liu, Q.; Yin, L.; Zhao, C.; Wang, J.; Wu, Z.; Lei, H.; Liu, Y.; Tian, B.; Zhang, Z.; Zhao, Z.; et al. Hybrid Mixed-Dimensional Perovskite/Metal-Oxide Heterojunction for All-in-One Opto-Electric Artificial Synapse and Retinal-Neuromorphic System. *Nano Energy* **2022**, *102*, 107686. [[CrossRef](#)]
115. Huang, X.; Li, Q.; Shi, W.; Liu, K.; Zhang, Y.; Liu, Y.; Wei, X.; Zhao, Z.; Guo, Y.; Liu, Y. Dual-Mode Learning of Ambipolar Synaptic Phototransistor Based on 2D Perovskite/Organic Heterojunction for Flexible Color Recognizable Visual System. *Small* **2021**, *17*, 2102820. [[CrossRef](#)] [[PubMed](#)]
116. Jo, C.; Kim, J.; Kwak, J.Y.; Kwon, S.M.; Park, J.B.; Kim, J.; Park, G.-S.; Kim, M.-G.; Kim, Y.-H.; Park, S.K. Retina-Inspired Color-Cognitive Learning via Chromatically Controllable Mixed Quantum Dot Synaptic Transistor Arrays. *Adv. Mater.* **2022**, *34*, 2108979. [[CrossRef](#)] [[PubMed](#)]
117. Shao, S.; Wang, S.; Li, M.; Xie, T.; Fang, Y.; Guo, P.; Chen, Z.; Zhao, J. 75 Kbit Printed Indium Oxide (IO)/Indium Gallium Zinc Oxide (IGZO) Heterojunction Photoelectric Synaptic Transistor Arrays for an Artificial Visual Memory System. *J. Mater. Chem. C* **2023**, *11*, 7019–7029. [[CrossRef](#)]
118. Kwon, S.M.; Cho, S.W.; Kim, M.; Heo, J.S.; Kim, Y.-H.; Park, S.K. Environment-Adaptable Artificial Visual Perception Behaviors Using a Light-Adjustable Optoelectronic Neuromorphic Device Array. *Adv. Mater.* **2019**, *31*, 1906433. [[CrossRef](#)]
119. Jin, C.; Liu, W.; Xu, Y.; Huang, Y.; Nie, Y.; Shi, X.; Zhang, G.; He, P.; Zhang, J.; Cao, H.; et al. Artificial Vision Adaption Mimicked by an Optoelectrical In₂O₃ Transistor Array. *Nano Lett.* **2022**, *22*, 3372–3379. [[CrossRef](#)]
120. Xie, S.; Wang, L.; Mao, X.; Cong, J.; Zhao, Y.; Chen, H. Brain Inspired Color Feature Selection Chip. *IEEE Photonics J.* **2022**, *14*, 1–9. [[CrossRef](#)]
121. Zhang, Y.; Wang, B.; Han, Z.; Shi, X.; Zhang, N.; Miao, T.; Lin, D.; Jiang, Z.; Liu, M.; Guo, H.; et al. Bidirectional Photoresponse in a Mixed-Dimensional MoS₂/Ge Heterostructure and Its Optic-Neural Synaptic Behavior for Colored Pattern Recognition. *ACS Photonics* **2023**, *10*, 1575–1582. [[CrossRef](#)]
122. Li, D.; Li, C.; Ilyas, N.; Jiang, X.; Liu, F.; Gu, D.; Xu, M.; Jiang, Y.; Li, W. Color-Recognizing Si-Based Photonic Synapse for Artificial Visual System. *Adv. Intell. Syst.* **2020**, *2*, 2000107. [[CrossRef](#)]
123. Dahiya, R.S.; Cattin, D.; Adami, A.; Collini, C.; Barboni, L.; Valle, M.; Lorenzelli, L.; Oboe, R.; Metta, G.; Brunetti, F. Towards Tactile Sensing System on Chip for Robotic Applications. *IEEE Sens. J.* **2011**, *11*, 3216–3226. [[CrossRef](#)]
124. Wang, Z.L.; Wu, W. Piezotronics and Piezo-Phototronics: Fundamentals and Applications. *Natl. Sci. Rev.* **2013**, *1*, 62–90. [[CrossRef](#)]
125. Kumar, M.; Singh, R.; Kang, H.; Kim, S.; Seo, H. An Artificial Piezotronic Synapse for Tactile Perception. *Nano Energy* **2020**, *73*, 104756. [[CrossRef](#)]
126. Xie, W.; Peng, W.; Wang, Y.; Li, F.; He, Y. On the Piezophototronic Effect in Heterojunction Photodiode with Type-II Energy Band: Theoretical Model for Anisotype Heterojunction. *Phys. Status Solidi RRL Rapid Res. Lett.* **2023**, *17*, 2300034. [[CrossRef](#)]
127. Peng, Y.; Que, M.; Lee, H.E.; Bao, R.; Wang, X.; Lu, J.; Yuan, Z.; Li, X.; Tao, J.; Sun, J.; et al. Achieving High-Resolution Pressure Mapping via Flexible GaN/ZnO Nanowire LEDs Array by Piezo-Phototronic Effect. *Nano Energy* **2019**, *58*, 633–640. [[CrossRef](#)]
128. Wang, C.; Gong, D.; Feng, P.; Cheng, Y.; Cheng, X.; Jiang, Y.; Zhang, D.; Cai, J. Ultra-Sensitive and Wide Sensing-Range Flexible Pressure Sensors Based on the Carbon Nanotube Film/Stress-Induced Square Frustum Structure. *ACS Appl. Mater. Interfaces* **2023**, *15*, 8546–8554. [[CrossRef](#)] [[PubMed](#)]

129. Cheng, X.; Cai, J.; Xu, J.; Gong, D. High-Performance Strain Sensors Based on Au/Graphene Composite Films with Hierarchical Cracks for Wide Linear-Range Motion Monitoring. *ACS Appl. Mater. Interfaces* **2022**, *14*, 39230–39239. [[CrossRef](#)]
130. Mahmud, M.A.P.; Tat, T.; Xiao, X.; Adhikary, P.; Chen, J. Advances in 4D-Printed Physiological Monitoring Sensors. *Exploration* **2021**, *1*, 20210033. [[CrossRef](#)]
131. Aygun, L.E.; Kumar, P.; Zheng, Z.; Chen, T.S.; Wagner, S.; Sturm, J.C.; Verma, N. Hybrid LAE-CMOS Force-Sensing System Employing TFT-Based Compressed Sensing for Scalability of Tactile Sensing Skins. *IEEE Trans. Biomed. Circuits Syst.* **2019**, *13*, 1264–1276. [[CrossRef](#)]
132. Qiao, Y.; Jian, J.; Tang, H.; Ji, S.; Liu, Y.; Liu, H.; Li, Y.; Li, X.; Han, F.; Liu, Z.; et al. An Intelligent Nanomesh-Reinforced Graphene Pressure Sensor with an Ultra Large Linear Range. *J. Mater. Chem. A* **2022**, *10*, 4858–4869. [[CrossRef](#)]
133. Kang, I.H.; Hong, M.T.; Bae, B.S. Capacitive Sensor Pixel Circuit with Single Transistor for Touch-Fingerprint Recognition Sensor. *Electron. Lett.* **2018**, *54*, 1212–1214. [[CrossRef](#)]
134. Zhang, C.; Li, S.; He, Y.; Chen, C.; Jiang, S.; Yang, X.; Wang, X.; Pan, L.; Wan, Q. Oxide Synaptic Transistors Coupled With Triboelectric Nanogenerators for Bio-Inspired Tactile Sensing Application. *IEEE Electron Device Lett.* **2020**, *41*, 617–620. [[CrossRef](#)]
135. Pang, Y.; Zhang, K.; Yang, Z.; Jiang, S.; Ju, Z.; Li, Y.; Wang, X.; Wang, D.; Jian, M.; Zhang, Y.; et al. Epidermis Microstructure Inspired Graphene Pressure Sensor with Random Distributed Spinosum for High Sensitivity and Large Linearity. *ACS Nano* **2018**, *12*, 2346–2354. [[CrossRef](#)] [[PubMed](#)]
136. Tian, X.; Liu, Z.; Luo, Z.; Wu, X.; Qiao, F.; Wang, X.; Li, G.; Wu, J.; Zhang, J.; Liu, Z.; et al. Dual-Mode Sensor and Actuator to Learn Human-Hand Tracking and Grasping. *IEEE Trans. Electron Devices* **2019**, *66*, 5407–5410. [[CrossRef](#)]
137. Yu, T.; Tao, Y.; Wu, Y.; Zhang, D.; Yang, J.; Liu, X. Self-Encapsulated Breathable Reduced Oxide Graphene-Coated Melamine Foam for Stress Sensing. *ACS Appl. Electron. Mater.* **2023**, *5*, 4624–4634. [[CrossRef](#)]
138. Jia, M.; Guo, P.; Wang, W.; Yu, A.; Zhang, Y.; Wang, Z.; Zhai, J. Tactile Tribotronic Reconfigurable P-n Junctions for Artificial Synapses. *Sci. Bull.* **2022**, *67*, 803–812. [[CrossRef](#)]
139. Khan, R.; Rehman, N.U.; Ilyas, N.; Sfina, N.; Barhoumi, M.; Khan, A.; Althubeiti, K.; Otaibi, S.A.; Iqbal, S.; Rahman, N.; et al. Threshold Switching in Nickel-Doped Zinc Oxide Based Memristor for Artificial Sensory Applications. *Nanoscale* **2023**, *15*, 1900–1913. [[CrossRef](#)] [[PubMed](#)]
140. Gong, G.; Gao, S.; Xie, Z.; Ye, X.; Lu, Y.; Yang, H.; Zhu, X.; Li, R.-W. A Visible Light-Triggered Artificial Photonic Nociceptor with Adaptive Tunability of Threshold. *Nanoscale* **2021**, *13*, 1029–1037. [[CrossRef](#)]
141. Yang, J.-H.; Mao, S.-C.; Chen, K.-T.; Chen, J.-S. Emulating Nociceptive Receptor and LIF Neuron Behavior via ZrO_x-Based Threshold Switching Memristor. *Adv. Electron. Mater.* **2023**, *9*, 2201006. [[CrossRef](#)]
142. Kim, Y.; Kwon, Y.J.; Kwon, D.E.; Yoon, K.J.; Yoon, J.H.; Yoo, S.; Kim, H.J.; Park, T.H.; Han, J.-W.; Kim, K.M.; et al. Nociceptive Memristor. *Adv. Mater.* **2018**, *30*, 1704320. [[CrossRef](#)]
143. Shrivastava, S.; Pratik, S.; Lin, A.S.; Tseng, T.Y. Emulating Synaptic and Nociceptive Behavior via Negative Photoconductivity of a Memristor. *IEEE Trans. Electron Devices* **2023**, *70*, 3530–3535. [[CrossRef](#)]
144. Bousoulas, P.; Tsiouostas, C.; Tsoukalas, D. Emulating Low Power Nociceptive Functionalities with a Forming-Free SiO₂/VO_x Conductive Bridge Memory with Pt Nanoparticles. *Appl. Phys. Lett.* **2022**, *120*, 253509. [[CrossRef](#)]
145. Xu, X.; Cho, E.J.; Bekker, L.; Talin, A.A.; Lee, E.; Pascall, A.J.; Worsley, M.A.; Zhou, J.; Cook, C.C.; Kuntz, J.D.; et al. A Bioinspired Artificial Injury Response System Based on a Robust Polymer Memristor to Mimic a Sense of Pain, Sign of Injury, and Healing. *Adv. Sci.* **2022**, *9*, 2200629. [[CrossRef](#)] [[PubMed](#)]
146. Xia, Q.; Qin, Y.; Qiu, P.; Zheng, A.; Zhang, X. A Bio-Inspired Tactile Nociceptor Constructed by Integrating Wearable Sensing Paper and a VO₂ Threshold Switching Memristor. *J. Mater. Chem. B* **2022**, *10*, 1991–2000. [[CrossRef](#)]
147. Niu, H.; Gao, S.; Yue, W.; Li, Y.; Zhou, W.; Liu, H. Highly Morphology-Controllable and Highly Sensitive Capacitive Tactile Sensor Based on Epidermis-Dermis-Inspired Interlocked Asymmetric-Nanocone Arrays for Detection of Tiny Pressure. *Small* **2020**, *16*, 1904774. [[CrossRef](#)]
148. Jang, S.; Jee, E.; Choi, D.; Kim, W.; Kim, J.S.; Amoli, V.; Sung, T.; Choi, D.; Kim, D.H.; Kwon, J.-Y. Ultrasensitive, Low-Power Oxide Transistor-Based Mechanotransducer with Microstructured, Deformable Ionic Dielectrics. *ACS Appl. Mater. Interfaces* **2018**, *10*, 31472–31479. [[CrossRef](#)] [[PubMed](#)]
149. Cao, Y.; Bu, T.; Fang, C.; Zhang, C.; Huang, X.; Zhang, C. High-Resolution Monolithic Integrated Tribotronic InGaZnO Thin-Film Transistor Array for Tactile Detection. *Adv. Funct. Mater.* **2020**, *30*, 2002613. [[CrossRef](#)]
150. Haniff, M.A.S.M.; Hafiz, S.M.; Huang, N.M.; Rahman, S.A.; Wahid, K.A.A.; Syono, M.I.; Azid, I.A. Piezoresistive Effect in Plasma-Doping of Graphene Sheet for High-Performance Flexible Pressure Sensing Application. *ACS Appl. Mater. Interfaces* **2017**, *9*, 15192–15201. [[CrossRef](#)]
151. Wang, M.; Tu, J.; Huang, Z.; Wang, T.; Liu, Z.; Zhang, F.; Li, W.; He, K.; Pan, L.; Zhang, X.; et al. Tactile Near-Sensor Analogue Computing for Ultrafast Responsive Artificial Skin. *Adv. Mater.* **2022**, *34*, 2201962. [[CrossRef](#)]
152. Fu, Y.; Chan, Y.-T.; Jiang, Y.-P.; Chang, K.-H.; Wu, H.-C.; Lai, C.-S.; Wang, J.-C. Polarity-Differentiated Dielectric Materials in Monolayer Graphene Charge-Regulated Field-Effect Transistors for an Artificial Reflex Arc and Pain-Modulation System of the Spinal Cord. *Adv. Mater.* **2022**, *34*, 2202059. [[CrossRef](#)]

153. Li, Y.; Yin, K.; Diao, Y.; Fang, M.; Yang, J.; Zhang, J.; Cao, H.; Liu, X.; Jiang, J. A Biopolymer-Gated Ionotronic Junctionless Oxide Transistor Array for Spatiotemporal Pain-Perception Emulation in Nociceptor Network. *Nanoscale* **2022**, *14*, 2316–2326. [[CrossRef](#)]
154. Tian, C.; Wei, L.; Jiang, J. MoS₂-Based Multiterminal Ionic Transistor with Orientation-Dependent STDP Learning Rules. *Solid-State Electron.* **2022**, *194*, 108386. [[CrossRef](#)]

Disclaimer/Publisher’s Note: The statements, opinions and data contained in all publications are solely those of the individual author(s) and contributor(s) and not of MDPI and/or the editor(s). MDPI and/or the editor(s) disclaim responsibility for any injury to people or property resulting from any ideas, methods, instructions or products referred to in the content.